



# Nano-Sized Iron Sulfide: Structure, Synthesis, Properties, and Biomedical Applications

Ye Yuan<sup>1,2,3</sup>, Liping Wang<sup>1,2</sup> and Lizeng Gao<sup>3,4\*</sup>

<sup>1</sup> Key Laboratory for Molecular Enzymology and Engineering, The Ministry of Education, Jilin University, Changchun, China, <sup>2</sup> School of Life Sciences, Jilin University, Changchun, China, <sup>3</sup> CAS Engineering Laboratory for Nanozyme, Institute of Biophysics, Chinese Academy of Sciences, Beijing, China, <sup>4</sup> Nanozyme Medical Center, School of Basic Medical Sciences, Zhengzhou University, Zhengzhou, China

Nano-sized iron sulfides have attracted intense research interest due to the variety of their types, structures, and physicochemical properties. In particular, nano-sized iron sulfides exhibit enzyme-like activity by mimicking natural enzymes that depend on an iron-sulfur cluster as cofactor, extending their potential for applications in biomedicine. The present review principally summarizes the synthesis, properties and applications in biomedical fields, demonstrating that nano-sized iron sulfides have considerable potential for improving human health and quality of life.

**Keywords:** nano-sized iron sulfide, structure, synthesis, enzyme-like activities, biomedical applications

## OPEN ACCESS

### Edited by:

Youhui Lin,  
Xiamen University, China

### Reviewed by:

Xian Chen,  
Shenzhen University, China  
Amitava Adhikary,  
Oakland University, United States

### \*Correspondence:

Lizeng Gao  
gaolizeng@ibp.ac.cn

### Specialty section:

This article was submitted to  
Nanoscience,  
a section of the journal  
Frontiers in Chemistry

**Received:** 19 May 2020

**Accepted:** 04 August 2020

**Published:** 10 September 2020

### Citation:

Yuan Y, Wang L and Gao L (2020)  
Nano-Sized Iron Sulfide: Structure,  
Synthesis, Properties, and Biomedical  
Applications. *Front. Chem.* 8:818.  
doi: 10.3389/fchem.2020.00818

## INTRODUCTION

With the development of nanotechnology (Li et al., 2019), nanomaterials have become a major resource for the development of novel therapeutic medicines and technologies designed to improve human health and the quality of life (Zhang and Webster, 2009; Esmaeili et al., 2020; Wang et al., 2020). In particular, due to their multiple functionality and excellent biocompatibility, iron-based nanomaterials are frequently used in the biomedical field, such as bioseparation, biosensors, magnetic resonance imaging (MRI), tumor hyperthermia, and drug delivery (Chen and Gu, 2017). In addition, recent studies have revealed that these nanomaterials have intrinsic enzyme-like properties (Gao et al., 2007; Xie et al., 2012; Xu et al., 2018), an important form of nanozyme representing a new generation of artificial enzyme (Wei and Wang, 2013; Dong et al., 2019; Liang and Yan, 2019). Currently, the majority of iron-based nanomaterials are iron oxide which possess excellent supraparamagnetic properties, with catalytic activity mimicking that of oxidoreductases, including peroxidase, catalase, superoxide dismutase, and oxidase (Gao et al., 2007; Liang and Yan, 2019). However, iron sulfide nanomaterials have not been comprehensively studied or used in the biomedical fields. Since O and S are congeneric elements, iron sulfide demonstrates similar physicochemical properties as iron oxide (Fu et al., 2019). In addition, the phases of iron sulfide in nature include mackinawite (FeS), pyrrhotite (Fe<sub>1-x</sub>S), pyrite (FeS<sub>2</sub>), and greigite (Fe<sub>3</sub>S<sub>4</sub>), etc., which exhibit more variability than iron oxide containing only Fe<sub>2</sub>O<sub>3</sub> and Fe<sub>3</sub>O<sub>4</sub>. The band gap in iron sulfide is smaller than that of iron oxide, leading to the former having more appropriate electron transfer and conductivity (Wadia et al., 2009; Jin et al., 2017; Zhang et al., 2018). Importantly, iron-sulfur clusters are important cofactors in many enzymes which serve as active centers for electron transfer in catalytic processes and respiratory chain reactions (Qi and Cowan, 2011). Therefore, it is anticipated that iron sulfide nanomaterials will display multiple functionalities and they have great potential in biomedical applications. Herein, we will summarize

the types, synthesis and properties of iron sulfide nanomaterials and emphasize their applications in biomedical and medical fields. This will provide a comprehensive understanding of iron sulfide nanomaterials and illustrate their considerable potential as novel multifunctional biomaterials in biomedical applications.

## TYPE AND STRUCTURE OF IRON SULFIDE

Solid phases of iron sulfides principally comprise FeS (mackinawite), Fe<sub>1-x</sub>S (pyrrhotite), FeS<sub>2p</sub> (pyrite), FeS<sub>2m</sub> (marcasite), Fe<sub>3</sub>S<sub>4</sub> (greigite), and Fe<sub>9</sub>S<sub>11</sub> (smythite). The content of iron within a biomaterial therefore influences its phase, shape, and physical and chemical properties. FeS naturally has a tetragonal structure, with each iron atom coordinated to four sulfurs. For Fe<sub>1-x</sub>S, a monoclinic hexagonal is present. FeS<sub>2p</sub> forms stable iron (II) disulfides with cubic structures. FeS<sub>2m</sub> differs from FeS<sub>2p</sub> as an orthorhombic metastable iron (II) disulfide, whilst Fe<sub>3</sub>S<sub>4</sub> is a cubic metastable Fe (II) Fe (III) sulfide. Hexagonal Fe<sub>9</sub>S<sub>11</sub> is related to the Fe<sub>1-x</sub>S phase (Rickard and Luther, 2007).

Reported crystal structures of iron sulfide are displayed in **Figure 1** (Fleet, 1971; Argueta-Figueroa et al., 2017). FeS possesses a tetragonal layered structure in which the iron atoms are linked through tetrahedral coordination to four equidistant sulfur atoms. A single iron atom is coordinated to four equidistant sulfur atoms. The distance of Fe-Fe is 2.5967 Å. In addition, Fe-Fe bonding is substantial in FeS. To assess the effects of van der Waals forces resulting from the S atoms, sheets including Fe are stacked along the C-axis. The spacing of these layers is 5 Å. The structure of Fe<sub>2</sub>S<sub>2</sub> is closed to FeS. The structure of FeS<sub>2</sub> is similar to that of NaCl in which S<sup>2-</sup> is located at the center of a cube. The cubic structure has a low symmetry. In addition, FeS<sub>2</sub> exhibits chirality through absorbed organic molecules. Fe<sub>3</sub>S<sub>4</sub> has an inverse spinel structure in which 8 Fe atoms are located at the tetrahedral A-sites and 16 Fe atoms are located at the B-sites of the octahedron. The unit cell of Fe<sub>3</sub>S<sub>4</sub> is 9.876 Å. In addition, the cubic structure of Fe<sub>3</sub>S<sub>4</sub> forms a closely packed array of S molecules linked by smaller Fe units (**Figure 1D**). It has been established that the Fe<sub>7</sub>S<sub>8</sub> structure is a hexagonal supercell (Fleet, 1971). The viable distribution of vacancy sites ideal for the base structure of NiAs was observed to describe the structure of Fe<sub>9</sub>S<sub>10</sub> (Elliot, 2010).

## SYNTHESIS OF NANO-SIZED IRON SULFIDES

Nano-sized iron sulfide encompasses a range of iron and sulfur compounds. Firstly, the range of chemical and biological methods for their production are discussed. In addition, the most reported synthesized methods for creating different phases of iron sulfide are presented in **Table 1**.

### Hydrothermal Synthesis

Thermal decomposition is the most commonly-used hydrothermal reaction for iron sulfide production. The typical solvothermal synthesis method of nFeS firstly involves the

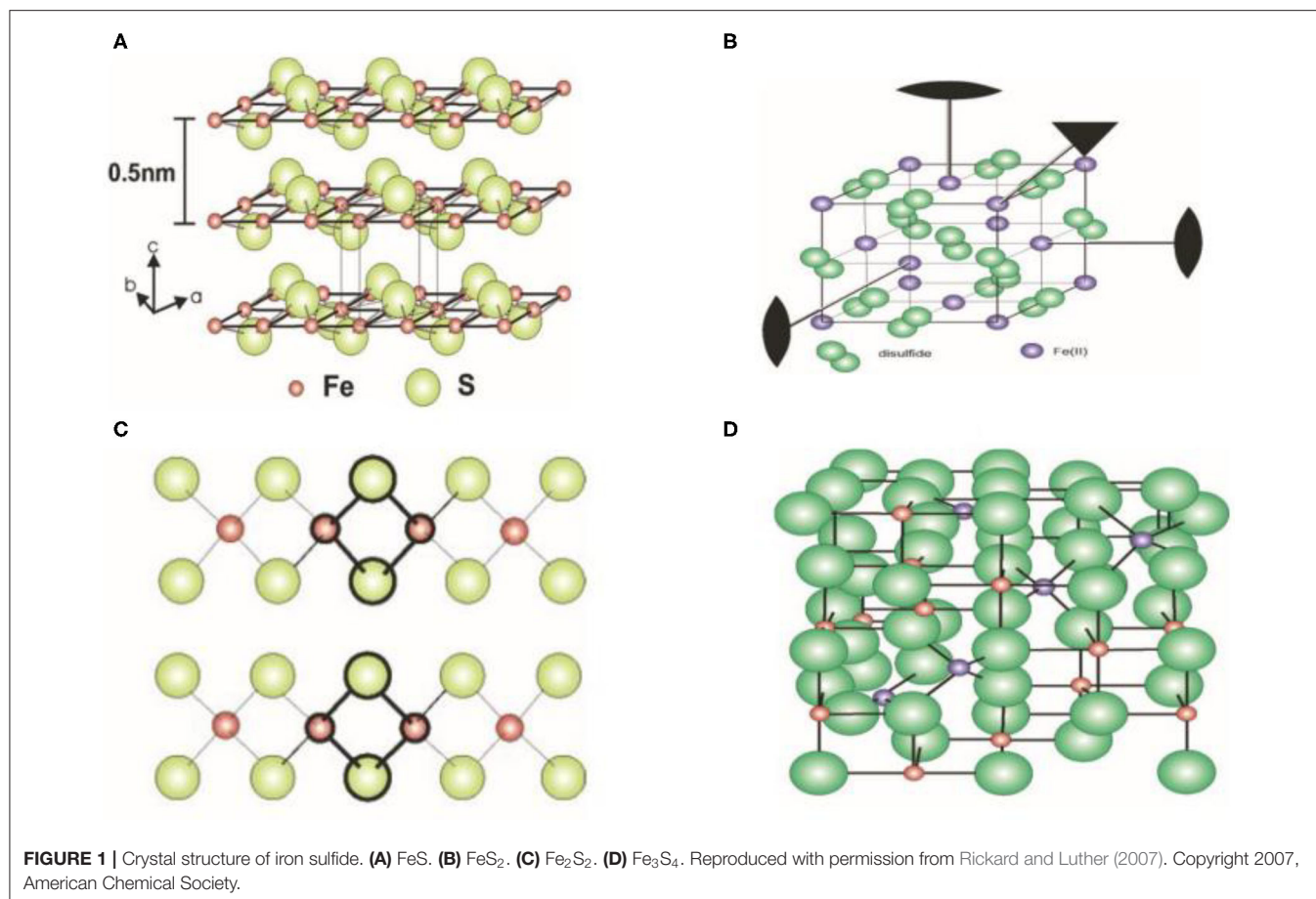
dissolution of FeCl<sub>3</sub>·6H<sub>2</sub>O in 40 mL of ethylene glycol. NaOAc and organosulfur compounds (allyl methyl sulfide, diallyl sulfide, diallyl trisulfide, diallyl disulfide, cysteine, cystine, glutathione (GSH), or methionine) are then added under continuous and vigorous stirring. The system was then sonicated for 10 min and transferred to a Teflon-lined stainless steel autoclave. The mixture was reacted at 200°C for 12 h and precipitates washed three times with ethanol and water. Finally, the products were dried at 60°C for 3 h (Xu et al., 2018). For FeS<sub>2</sub>, the single source molecular precursor Fe<sup>3+</sup> diethyl dithiophosphate forms an aqueous solution through the reaction of FeCl<sub>3</sub> and (C<sub>2</sub>H<sub>5</sub>O)<sub>2</sub>P(S)NH<sub>4</sub>, with hexadecyltrimethylammonium bromide (CTAB) added as a surfactant and reacted with a single precursor [(C<sub>2</sub>H<sub>5</sub>O)<sub>2</sub>P(S)]<sub>3</sub>Fe (Wadia et al., 2009). For FeS, FeCl<sub>3</sub>·6H<sub>2</sub>O was dissolved in ultrapure water with ethanolamine and thiourea added to the solution. After stirring for 25 min, the mixture was added to a Teflon lined autoclave and reacted at 180°C for 12 h. The synthesis of Fe<sub>3</sub>S<sub>4</sub> differs from that of FeS. FeCl<sub>3</sub>·6H<sub>2</sub>O, ethylene glycol, thiourea and H<sub>2</sub>O<sub>2</sub> were mixed and reacted at 180°C for 18 h in the presence of the capping agent polyvinyl pyrrolidone (PVP) to prevent excessive growth and aggregation of the nanoparticles (NPs) (Moore et al., 2019). Fe<sub>1-x</sub>S single crystals were then synthesized through a hydrothermal method by the addition of K<sub>0.8</sub>Fe<sub>1.6</sub>S<sub>2</sub> crystals, Fe powder, NaOH, and thiourea in deionized water, which was reacted at 120°C for 3–4 days (Guo et al., 2017). Ionic liquids that form extended hydrogen bond systems were then used to form higher structures in the base of the hydrothermal process, as reported by Zheng and colleagues when changing the structure of Fe<sub>3</sub>S<sub>4</sub> (Ma et al., 2010). Generally speaking, the product obtained by the hydrothermal method has better dispersibility and controllability, but iron oxide impurities can also appear during the synthesis of iron sulfide. Meanwhile, multiphase iron sulfide appears to occur easily, as assessed by X-ray diffraction (XRD) patterns for hydrothermally-synthesized samples.

### Microwave Production

The principal advantages of microwave-assisted methods, compared with conventional heating include its reduced reaction time, smaller particle size distribution, and higher purity. Ethylene glycol is a solvent suitable for microwave-assisted methods owing to its relatively high dipole moment. For FeS<sub>2</sub> microspherulites, FeSO<sub>4</sub>·7H<sub>2</sub>O, PVP-K30 and S powder in ethylene glycol can be reacted by microwave in an N<sub>2</sub> atmosphere (Li M. et al., 2011). Although this emerging technique may be more desirable it should be noted that the aggregation phenomenon does not appear to be improved.

### Co-precipitation

Chemical co-precipitation does not introduce impurities. The operation is performed under mild conditions and is typically synthesized using Fe<sub>3</sub>S<sub>4</sub> methods, in which iron (II) sulfate heptahydrate and sodium sulfide are dissolved in ultrapure deionized water. The solution was then added dropwise to acetic acid to adjust the pH to 3.0, followed by stirring for several minutes. The reaction was prepared under an N<sub>2</sub> atmosphere (Chang et al., 2011). In addition, green synthesis was achieved



in a continuous stirred-tank reactor (Simeonidis et al., 2016). As previously reported, the conditions of synthesis required by co-precipitation are harsher than those of other methods, and the products obtained may show poor homogeneity.

### High Temperature Chemical Synthesis

Chemical synthesis methods using high temperatures have been reported for FeS<sub>2</sub>. Briefly, iron (II) acetylacetonate (Fe(acac)<sub>2</sub>), trioctylphosphine oxide (TOPO) and oleyamine (OLA) were mixed and degassed at 110°C for 1 h under a vacuum. The mixture was then rapidly heated to 220°C for 1 h under vigorous magnetic stirring in the presence of nitrogen. Sulfur was then quickly injected into the solution, which was heated to 220°C for 1 h. Once the solution cooled, ethanol was added to the precipitate to develop the FeS<sub>2</sub> nanoplates (Bi et al., 2011). Synthesis methods for Fe<sub>1-x</sub>S and Fe<sub>3</sub>S<sub>4</sub> have also been reported. The rapid injection method has been used to reduce the size of Fe<sub>3</sub>S<sub>4</sub> (Beal et al., 2012). This method of synthesis is highly sensitive to the experimental conditions.

### Sonochemical Synthesis

As a convenient and stable synthetic method, Bala and colleagues described specific FeS' sonochemical synthesis. Firstly, sodium sulfide was dissolved in double distilled water. FeSO<sub>4</sub>·7H<sub>2</sub>O was then independently dissolved in a solution of double

distilled water and polyethylene glycol (1:1). The sodium sulfide solution contained a drop of Triton-X surfactant which was added dropwise to the above solution while being continuously sonicated for 30 min. PVP was then added and the system was mixed via ultrasound for a further 30 min (Ahuja et al., 2019).

### Other Chemical Methods

Some unusual synthetic chemical methods have been reported. The low temperature synthesis of FeS<sub>2</sub> nanoparticles was described in 2014 (Srivastava et al., 2014a). Briefly, FeCl<sub>3</sub> and sodium polysulfide (Na<sub>2</sub>S<sub>x</sub>) were mixed in pH 5.6 acetate buffer in an anaerobic environment. The black solution then was reacted in a 90–100°C oil bath for 4 h to produce a grayish FeS<sub>2</sub> product. Flux methods were then used to synthesize 1D Fe<sub>7</sub>S<sub>8</sub>. The reaction was conducted within a furnace at 750–850°C (Kong et al., 2005). FeS can also be created in a biological system (Mei and Ma, 2013).

### Biomineralization

The bio-synthesis of iron sulfide using microorganisms is superior for biomedical applications (Li X. et al., 2011). When microorganisms interact with target ions, they are transported into microbial cells to form NPs in the presence of specific enzymes. In addition to the advantages of green synthesis, biological methods improve the biocompatibility of iron sulfide.

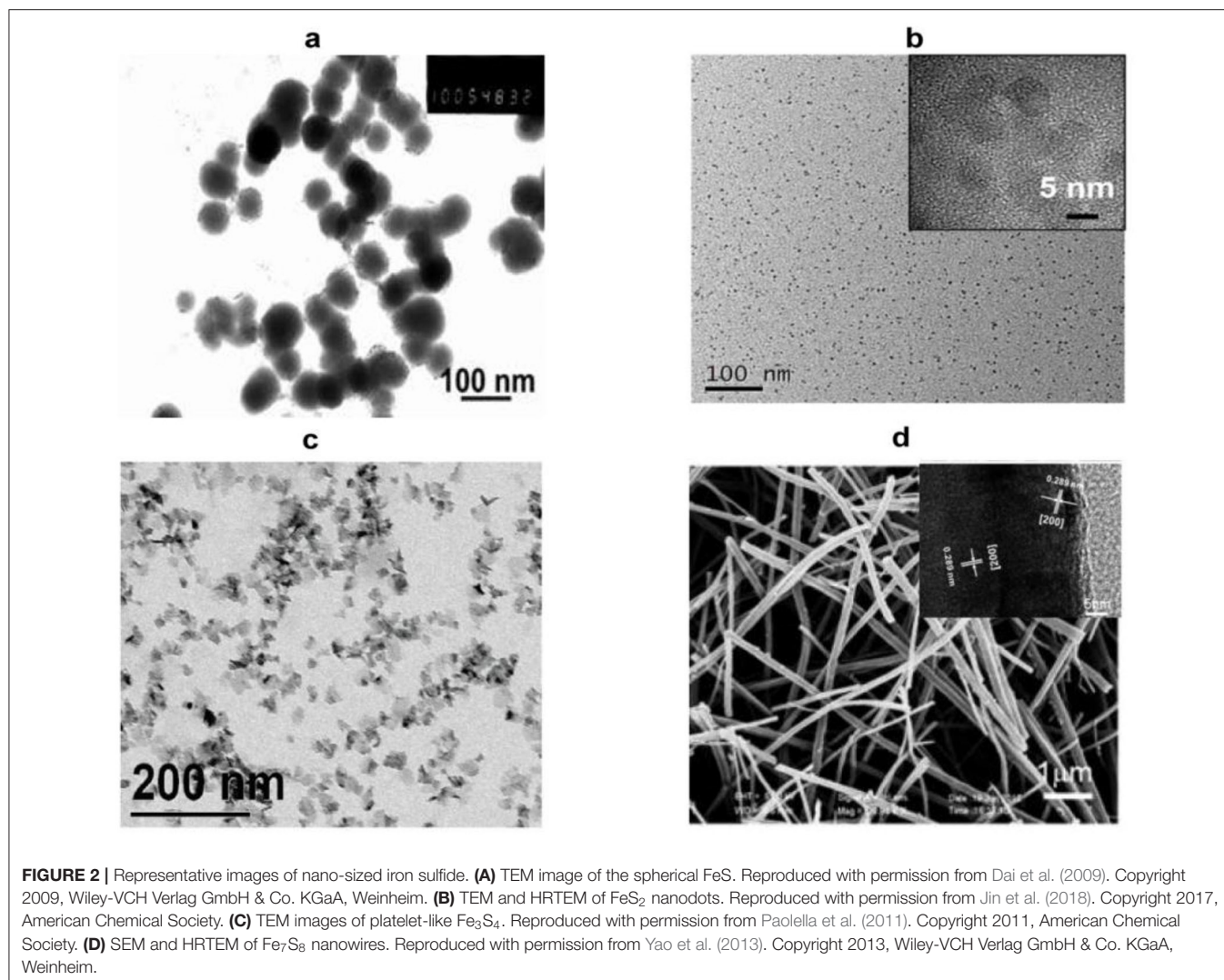
**TABLE 1** | Appearances, sizes and lattice spaces of iron sulfide.

Phase	Method	Appearances	Size (nm)	Lattice space (nm)	References	
FeS	High temperature chemical synthesis	Nanoplates	32–36	0.286	Yang et al., 2015	
	Sonochemical synthesis	Spherical	6–20		Ahuja et al., 2019	
	Biosystem	Spherical	30–50		Mei and Ma, 2013	
	Hydrothermal synthesis	Pomegranate flower-like	3,000		Jin et al., 2017	
	Co-precipitation Co-precipitation	Regular spherical Nanoparticles	50 60–80 102 (DLS)		Dai et al., 2009; Agnihotri et al., 2020	
	Biom mineralization	Spherical	2	Watson et al., 1999		
FeS <sub>2</sub>	High temperature chemical synthesis	Cubic	60–200	0.269	Bi et al., 2011	
	Ionic liquid-modulated synthesis	Hexagonal nanoplates	12,000 30 (side length)		Ma et al., 2010	
	Hydrothermal synthesis	Quasi-cubic nanocrystal	Over 100		Wadia et al., 2009	
	Microwave	Big particles	200		Kim and Batchelor, 2009	
	Hydrothermal synthesis	Uniform nanowires	40–60		Kar and Chaudhuri, 2004	
	Hydrothermal synthesis	Nanorods	40–100		Kar and Chaudhuri, 2004	
	Hydrothermal synthesis	Nanoribbons	100–250		0.313	Kar and Chaudhuri, 2004
	Microwave	Monodisperse microspherulites	2,400		0.27	Li M. et al., 2011
	Biom mineralization	Nanodots	7		Jin et al., 2018	
	Low temperature synthesis	Hexagonal	600–700		Srivastava et al., 2014b	
Fe <sub>3</sub> S <sub>4</sub>	Hydrothermal synthesis	Spherical	76 165 (DLS)	0.298	Ding et al., 2016	
	Hydrothermal synthesis Hydrothermal synthesis	Plates Dispersible nanoparticles	2000–5000 17.7		Fu et al., 2019; Moore et al., 2019	
	Hydrothermal synthesis Hydrothermal synthesis Hydrothermal synthesis	Nanocrystals Hexagonal nanoplates Monodisperse nanocrystals	2.5–4.5 12,000 30 (side length) 100 175 (DLS)		Vanitha and O'Brien, 2008; Ma et al., 2010; He et al., 2013	
	Co-precipitation Co-precipitation Co-precipitation	Irregular particles Nanoparticles Platelet-like	50–100 20–35 10–20		0.572	Chang et al., 2011; Paoletta et al., 2011; Simeonidis et al., 2016
	High temperature chemical synthesis	Spherical	5		0.25	Beal et al., 2012
Fe <sub>7</sub> S <sub>8</sub>	Hydrothermal synthesis	Spherical	5.6	0.289	Vanitha and O'Brien, 2008	
	Flux	hedgehog-like	10,000		Kong et al., 2005	
	Flux	Nanorods	200 1500–2000 (length)		Kong et al., 2005	
	Flux	Nanosheets	Smaller than 100 (thickness)		Kong et al., 2005	
	Hydrothermal synthesis	Nanowires			Yao et al., 2013	
	High temperature chemical synthesis	Nanosheets	5,000 500 (thickness)		Wang et al., 2013	

The particles generated have higher catalytic reactivity and a greater surface area. Previous studies have reported that FeS<sub>2</sub>, Fe<sub>3</sub>S<sub>4</sub>, and FeS NPs can be produced by microorganisms. For the biom mineralization of Fe<sub>3</sub>S<sub>4</sub> and FeS<sub>2</sub>, a magnetotactic bacterium has been described (Mann et al., 1990). In 1995, FeS materials were produced by sulfate-reducing bacteria grown on iron containing substrates (Watson et al., 1995). Bazylinski and colleagues also reported the formation of Fe<sub>3</sub>S<sub>4</sub> using non-cultured magnetotactic bacteria (Lefèvre et al., 2010). Sulfate-reducing bacteria were able to produce Fe<sub>1-x</sub>S as reported by Charnock and colleagues (Watson et al., 2000). NPs were subsequently formed at the surface by the microorganisms and as such, the porous structure of the iron sulfide NPs failed to prevent normal metabolism. These studies verified the utility of this method for efficient NP production. Chemical biom mineralization methods have also been used to synthesize FeS<sub>2</sub> and FeS Quantum dots (QDs) (Jin et al., 2018; Yang et al., 2020).

## Iron Sulfide Modifications

Bare nanocrystal cores have an unstable structure that is prone to photochemical degradation. However, those that are unmodified display higher toxicity. As such, biocompatible moieties are essential as they serve as caps for nanomaterials, including polyethylene glycol (PEG), silica, lactose, citrate, and dextran (Simeonidis et al., 2016; Mofokeng et al., 2017). Previous studies have reported the synthesis, characterization, cytotoxicity and biodistribution of FeS/PEG nanoplates *in vivo* (Yang et al., 2015). An adsorption-reduction method was used to load silver onto the surface of 3-aminopropyltriethoxysilanemodified 3-aminopropyl triethoxysilane (APTES)-modified Fe<sub>3</sub>S<sub>4</sub> particles, achieving the preparation of magnetic composite nanoparticles of Fe<sub>3</sub>S<sub>4</sub>/Ag (He et al., 2013). However, modifications also led to adverse effects. For example, the modification of CTAB inhibited the growth of nano Fe<sub>3</sub>S<sub>4</sub> (Simeonidis et al., 2016).



## Characterization of Iron Sulfide

Detailed characterization is required to confirm the synthesis of iron sulfide. Scanning electron microscopy (SEM) and transmission electron microscopy (TEM) can be used to image surface morphology. These represent the most direct and commonly-used methods to assess the microstructure, size, and dispersion of the materials. Differences in the synthetic methods have presented variations in TEM/SEM imaging, including within the same phase. For FeS, nanoplates, spherical nanoparticles, and pomegranate flower-like shapes have been reported. FeS<sub>2</sub> exists as large particles, cubic nanocrystals, monodisperse microspherulites, spherical and hexagonal nanoribbons, and nanorods. Typical images of iron sulfide are shown in **Figure 2**. **Table 1** reports the most common morphology and size of FeS, FeS<sub>2</sub>, Fe<sub>3</sub>S<sub>4</sub>, and Fe<sub>7</sub>S<sub>8</sub>. Lattice spaces are measured to judge the crystallinity of the materials. The reported lattice spaces of the iron sulfides are summarized in **Table 1**. The composition, content, and structure of a substance can be analyzed, measured, and inferred using Ultraviolet-visible

(UV-Vis) spectrometry and the absorption of UV and visible light. According to previous studies, the UV absorption peaks of FeS are 285 nm and 500 nm (**Table 2**). Information on the composition of the materials and the structure and/or morphology of the atoms or molecules inside the materials can be obtained by XRD analysis. XRD is the most direct indicator of whether a crystal is pure and so represents a convenient system to analyze synthesized materials. JCPDS cards are used to contrast and analyze unknown crystals. JCPDS cards of FeS (JCPDS card No. 15-0037 and 75-0602), FeS<sub>2</sub> (JCPDS card No. 03-065-1211, 89-3057, 65-3321, and 42-130), Fe<sub>3</sub>S<sub>4</sub> (JCPDS card No. 16-0713, 89-1998, and 16-0073) and Fe<sub>7</sub>S<sub>8</sub> (JCPDS card No. 25-0411 and 76-2308) are listed in **Table 2**. For iron sulfide nanomaterials, the X-ray photoelectron spectroscopy (XPS) of Fe and S are essential. FeS materials are presented in **Table 2** (Fe 2p: 2p<sub>3/2</sub> (711.4 eV), 2p<sub>1/2</sub> (724.9 eV), S 2p: 2p<sub>3/2</sub> (161.1 eV), 2p<sub>1/2</sub> (166.0 eV)), FeS<sub>2</sub> (Fe 2p: 2p<sub>3/2</sub> (707.0 eV), 2p<sub>1/2</sub> (720.0 eV), S 2p: 2p<sub>3/2</sub> (162.3 eV), 2p<sub>1/2</sub> (163.5 eV)), Fe<sub>3</sub>S<sub>4</sub> (Fe 2p: 2p<sub>3/2</sub> (711.0 eV), S 2p: 2p<sub>3/2</sub> (161.0 eV), 2p<sub>1/2</sub> (162.5 eV)), Fe<sub>7</sub>S<sub>8</sub> (Fe

**TABLE 2** | UV-VIS, XPS and XRD of iron sulfide.

Phase	UV-Vis peak (nm)	XPS	XRD	References
FeS	500 285 A broad absorption in (400–700 nm)	Fe 2p 2p <sub>3/2</sub> (711.4 eV) 2p <sub>1/2</sub> (724.9 eV) S 2p 2p <sub>3/2</sub> (161.1 eV) 2p <sub>1/2</sub> (166.0 eV)	JCPDS card No.15-0037 JCPDS card No.75-0602	Guo et al., 2016; Jin et al., 2017; Ahuja et al., 2019; Agnihotri et al., 2020
FeS <sub>2</sub>		Fe 2p 2p <sub>3/2</sub> (707.0 eV) 2p <sub>1/2</sub> (720.0 eV) S 2p 2p <sub>3/2</sub> (162.3 eV) 2p <sub>1/2</sub> (163.5 eV)	JCPDS card No.03-065-1211 JCPDS card No.89-3057 JCPDS card No.65-3321 JCPDS card No.42-1340	Kar and Chaudhuri, 2004; Wadia et al., 2009; Li M. et al., 2011; Gan et al., 2016
Fe <sub>3</sub> S <sub>4</sub>		Fe 2p 2p <sub>3/2</sub> (711.0 eV) S 2p 2p <sub>3/2</sub> (161.0 eV) 2p <sub>1/2</sub> (162.5 eV)	JCPDS card No.16-0713 JCPDS card No.89-1998 JCPDS card No.16-0073	Ma et al., 2010; Chang et al., 2011; Paolella et al., 2011; Beal et al., 2012; Feng et al., 2013; He et al., 2013; Ding et al., 2016; Moore et al., 2019
Fe <sub>7</sub> S <sub>8</sub>		Fe 2p 2p <sub>3/2</sub> (709.9 eV) (711.6 eV) S 2p 2p <sub>3/2</sub> (163.5 eV) 2p <sub>1/2</sub> (164.7 eV)	JCPDS card No. 25-0411 JCPDS card No.76-2308 JCPDS card No.71-0647	Kong et al., 2005; Vanitha and O'Brien, 2008; Wang et al., 2013; Yao et al., 2013; Jin et al., 2019

2p: 2p<sub>3/2</sub> (709.9 eV), (711.6 eV), S 2p: 2p<sub>3/2</sub> (163.5 eV), 2p<sub>1/2</sub> (164.7 eV)). Fourier transform infrared (FTIR) spectroscopy can be used to detect functional groups in a complex mixture and so is therefore essential to the characterization of modified iron sulfide. Previous studies have provided FTIR spectra, showing successful modifications by APTES on the surface of the Fe<sub>3</sub>S<sub>4</sub> nanoparticles (He et al., 2013). Fe<sub>7</sub>S<sub>8</sub>/N-C nanohybrids were prepared for FeMOF and FeMOF-S and analyzed by FTIR (Jin et al., 2019). In addition, energy dispersive spectroscopy (EDS) (Paolella et al., 2011; Ding et al., 2016; Guo et al., 2016), dynamic light scattering (DLS) (He et al., 2013; Ding et al., 2016), Raman spectroscopy (Gan et al., 2016; Guo et al., 2016), selected area electron diffraction (SAED) (Kar and Chaudhuri, 2004), X-ray absorption fine structure (XAFS) (Feng et al., 2013), differential scanning calorimetry (DSC) and thermogravimetric analysis (TGA) (Jin et al., 2019), nitrogen adsorption–desorption isotherms and pore size distribution (Guo et al., 2016) analysis of iron sulfide have been reported as characterization systems.

## CHARACTERISTICS OF NANO-SIZED IRON SULFIDES

In addition to both the physical and chemical properties, characteristics include the structure, solubility, stability, reactivity, magnetic properties, and photothermal properties of the products.

### Solubility

The major forms of nano-sized iron sulfides are solid precipitates which have poor solubility in water. However, Rickard et al. revealed that sedimental FeS can dissolve at  $c(S^{2-}) \leq 10^{-5.7}$  M to form Fe<sup>2+</sup>. The solubility can be increased in an alkaline as opposed to neutral environment (Rickard, 2006). FeS does not dissolve in HCl, meaning it cannot be removed with HCl (Rickard and Luther, 2007). According to previous studies, the  $K_{sp}$  of FeS<sub>2</sub> was  $10^{-16.4}$  at 25°C. The solubility products of various iron sulfides were assessed and resulted in consensus values for the pKs (FeS:  $3.6 \pm 0.2$ ; FeS<sub>2</sub>  $16.4 \pm 1.2$ ; Fe<sub>3</sub>S<sub>4</sub>  $4.4 \pm 0.1$ ; Fe<sub>7</sub>S<sub>8</sub>  $5.1 \pm 0.1$ ). This improved our understanding of the

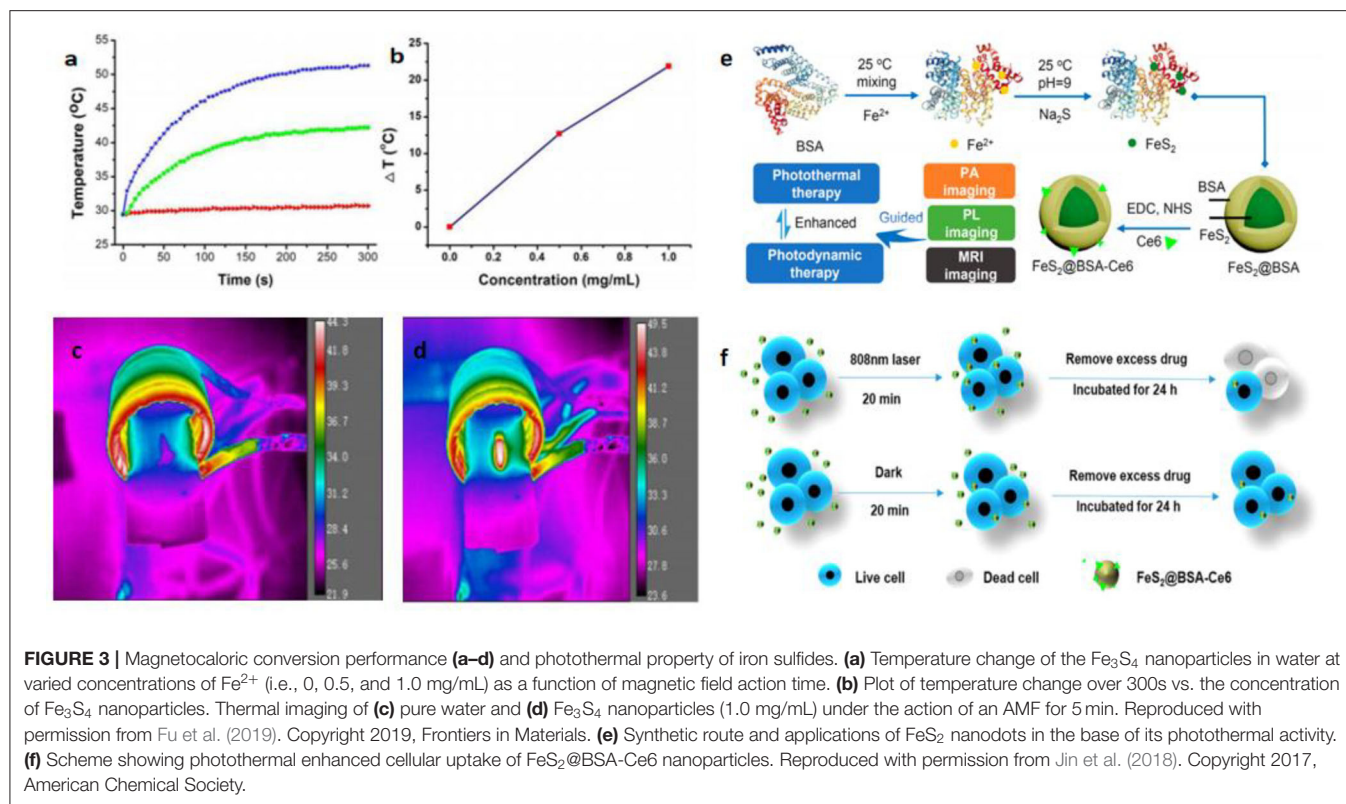
solubility of iron sulfide in both synthetic and natural water at room temperature (Davison, 1991).

### Stability

FeS is stable within the P-T range of the Martian core (Kavner et al., 2001). Understanding the relationship between the stability of iron sulfide and its chemical environment is of key importance. Once iron sulfide is formed, its structure is reversible. Studies have examined the stability of FeS<sub>2</sub> in different temperatures and the concentrations of absorbed water on the surface. Temperature has little effect on the morphology of FeS<sub>2</sub> under low absorbed water concentrations. However, at above 90 K, the conversion from an octahedral structure to a cubic shape is promoted. At higher concentrations of water, the dependence on temperature is more apparent (Barnard and Russo, 2009). The latter study established that functions of the surface ligands affect the stability of FeS<sub>2</sub> (FeS<sub>2</sub> nanorods synthesized in laboratory) (Barand and Russo, 2009). The stability of FeS contributed to low energy excitation from Fe d to S-S<sub>o</sub>\*p (Zhang et al., 2018). Fe<sub>3</sub>S<sub>4</sub> was observed at 200°C for 30 h then it transformed to FeS<sub>2</sub> over time (Gao et al., 2015).

### Reactivity

Iron sulfide is highly reactive to N<sub>2</sub> and H<sub>2</sub>S. This reaction occurs at room temperature and the adsorption of N<sub>2</sub> is dependent on the surface FeS and on the electronic state of N<sub>2</sub>. A decrease in absorbed N<sub>2</sub> and H<sub>2</sub>S could be explained by the formation of ammonia (Kasting, 1993). The reactivity of Fe<sub>7</sub>S<sub>8</sub> is similar to FeS (Niño et al., 2018). The presence of both Au<sup>1+</sup> and Au atoms has been observed on the surface of FeS<sub>2</sub>. Au deposition increased at higher pH and temperatures. The reactivity of Au<sup>1+</sup> sulfides with FeS<sub>2</sub> have also been investigated (Scaini et al., 1998). The reactivity of FeS<sub>2</sub> using gaseous H<sub>2</sub>O and O<sup>2-</sup> was similarly reported. Gaseous H<sub>2</sub>O leads to the formation of iron hydroxides on FeS<sub>2</sub>. A sequence of different exposures also leads to the formation of a range of products (SO<sub>4</sub><sup>2-</sup>, Fe(OH)<sub>3</sub>) (Usher et al., 2005). Recently, FeS<sub>2</sub> was shown to be a potential nanomaterial for prebiotic chemistry due to its highly reactive surface that drives amino acid adsorption (Ganbaatar et al., 2016). Among the most common probes, water molecules have been used to explore



the reactivity of  $\text{FeS}_2$  (De Leeuw et al., 2000). The different phases of iron sulfide display a wide range of reactivities to chlorinated solvents. Conditions including pH, sulfide concentrations, metal ions, and natural organic matter can affect the reaction kinetics of the degradation of chlorinated solvents (He et al., 2015). The interaction of  $\text{FeS}$ ,  $\text{Fe}_3\text{S}_4$  and  $\text{CO}_2$  have also been reported. The charge transfer on  $\text{FeS}$  can also effectively activate  $\text{CO}_2$ , whilst  $\text{Fe}_3\text{S}_4$  is unreactive to  $\text{CO}_2$  (SantosCarballal et al., 2017).

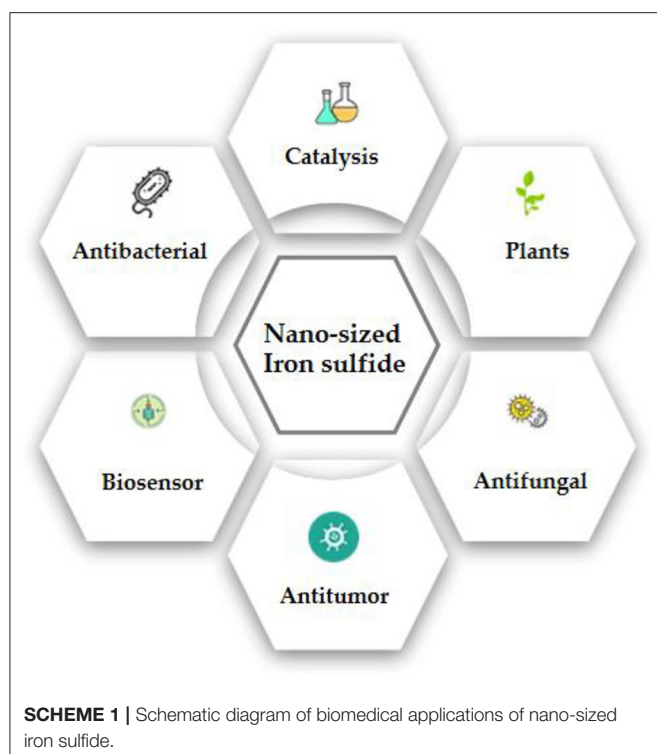
## Magnetic Properties

Nanomaterials with magnetic properties have numerous applications, including magnetocaloric therapies, as MRI agents, magnetic separation materials, and magnetic carriers. The discovery of their magnetic properties led to the identification of iron sulfide phases. The ferromagnetism of  $\text{Fe}_7\text{S}_8$  can be explained by  $\text{Fe}^{3+}$  ions with excess sulfur (Yosida, 1951). The magnetic susceptibility  $\chi$  of natural  $\text{FeS}_2$  was found to be  $64 \times 10^{-6} 68 \times 10^{-6} \text{ cm}^3 / \text{moles}$  between 4.2 and 380 K (Mohindar and Jagadeesh, 1979). Magnetic ordering in  $\text{FeS}$  was inferred and used to prove strong itinerant spin fluctuations.  $\text{FeS}$  can also be used as a superconductor (Kwon et al., 2011). Even when the structure of  $\text{FeS}$  is changed from troilite to the MnP-type under high pressure, the antiferromagnetic properties are preserved until the monoclinic structure is formed (Ono, 2007). The magnetic moment then disappears and yetragonal-phase  $\text{FeS}$  ( $T_c$ : 5K) was observed for the same structure as the superconductor  $\text{FeSe}$  ( $T_c$ : 8 K) (Kuhn et al., 2016).  $\text{Fe}_3\text{S}_4$  displays high  $M_{rs}/\chi$ , ( $M_{rs}/\chi$ : the saturation isothermal remnant magnetization:

magnetic susceptibility) and its  $M_{rs}/M_s$  (hysteresis ratios) and  $B_{cr}/B_c$  are 0.5 and 1.5 ( $M_s$ : saturation magnetization;  $B_c$ : the coercive force;  $B_{cr}$ : the coercivity of remanence).  $\text{Fe}_3\text{S}_4$  also displays unique high-temperature properties, with a clear drop in magnetization from 270 to 350°C (Roberts, 1995). Synthesized  $\text{Fe}_3\text{S}_4$  contains various crystals from small superparamagnetic grains (non-remnance) to large multi-domain grains (Snowball, 1991). The magnetic hysteresis properties of  $\text{Fe}_7\text{S}_8$  have also been studied (Menyeh and O'Reilly, 1997). The relationship between structure and magnetic properties has been reported within variable temperatures. Magnetic transitions occurred within the transformation of the structure (Powell et al., 2004). The magnetocaloric conversion ability of  $\text{Fe}_3\text{S}_4$  nanoparticles has been measured under an alternating magnetic field (AMF). Meanwhile, the excellent physical and chemical properties provide magnetothermal thrombolytic ability in medical applications (Fu et al., 2019; Figure 3).

## Photothermal Properties

Photothermal therapy (PTT) has attracted considerable attention in recent years. The mechanism of PTT results mainly from photo-absorbing nanomaterials that generate heat through continuous laser irradiation, destroying cancer cells, but causing no damage to healthy tissue. It is therefore necessary to pay attention to the photothermal properties of iron sulfide. PEGylated  $\text{FeS}$  ( $\text{FeS-PEG}$ ) nanoplates exhibit high near infrared (NIR) absorbance. Using Infrared (IR) thermal imaging, the



temperature can reach 70°C within 5 min. Meanwhile, FeS-PEG displays stronger photothermal conversion efficiency than other known iron oxides (Yang et al., 2015). Ultrasmall FeS<sub>2</sub> nanodots have also been synthesized and have been shown to be useful for photodynamic therapy. Chlorin e6 (Ce6) was used to conjugate FeS<sub>2</sub> in the presence of the template bovine serum albumin (BSA). FeS<sub>2</sub>@BSA-Ce6 nanodots (7 nm) demonstrated good results in *in vivo* photoacoustic (PA) imaging, MRI and enhanced cellular uptake (Jin et al., 2018; Figure 3).

## Biomedical Applications

To-date, a variety of biomedical applications of iron sulfide (catalysts, antibacterial agents, cancer therapies, drug delivery systems, thrombolytic agents, biosensors, antifungal agents, seed improvers in phyto-applications) and their functional mechanisms have been summarized (Scheme 1).

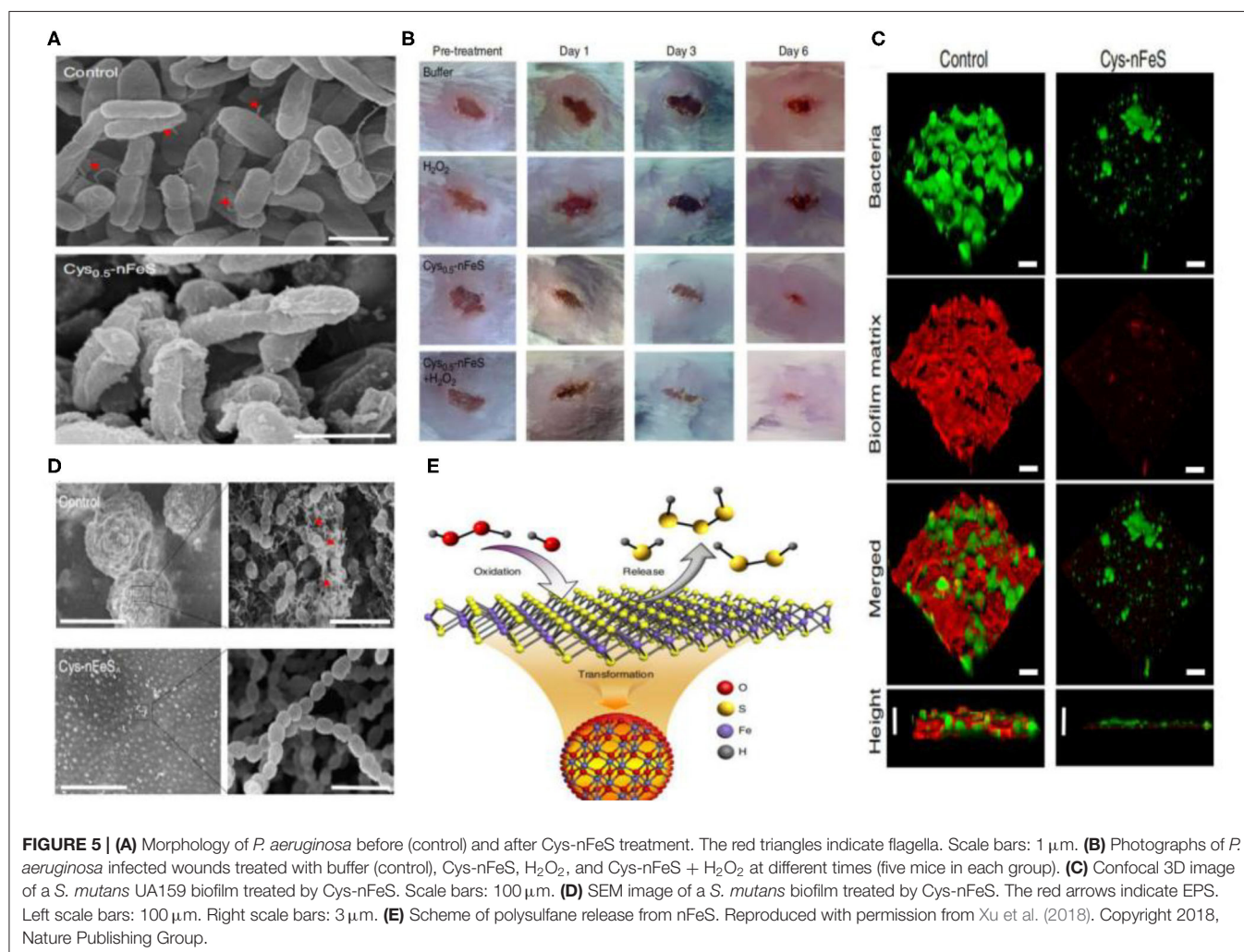
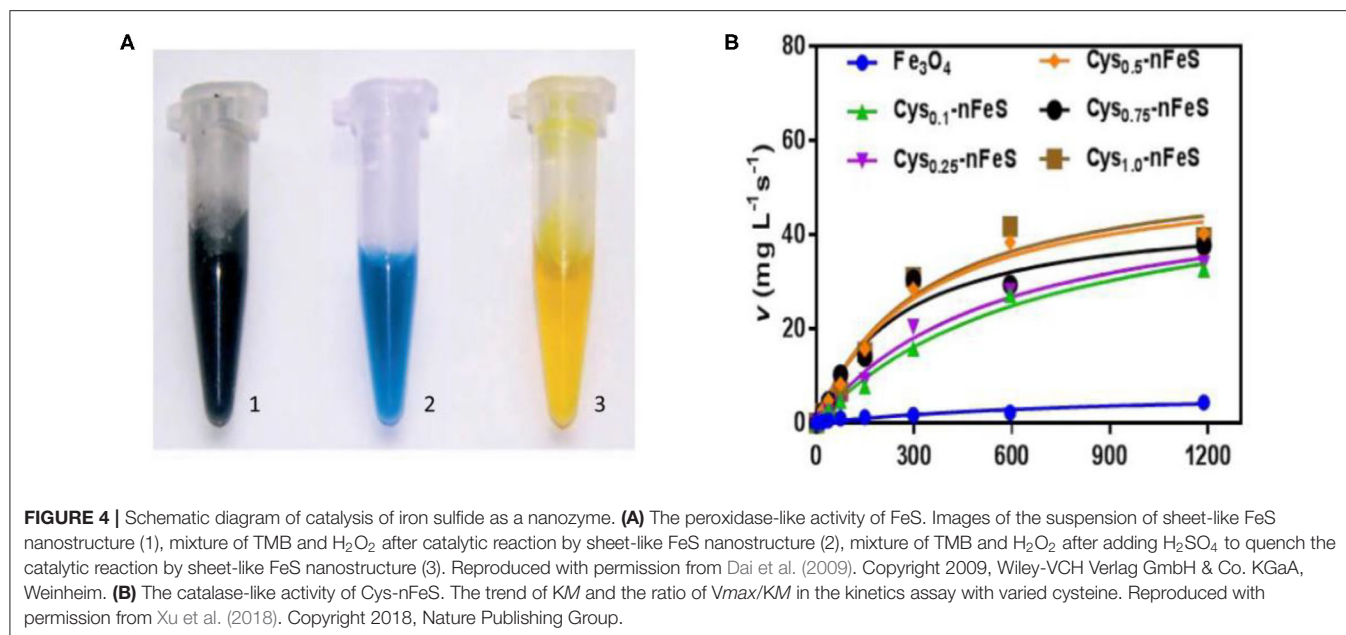
## Enzyme-Like Catalysis

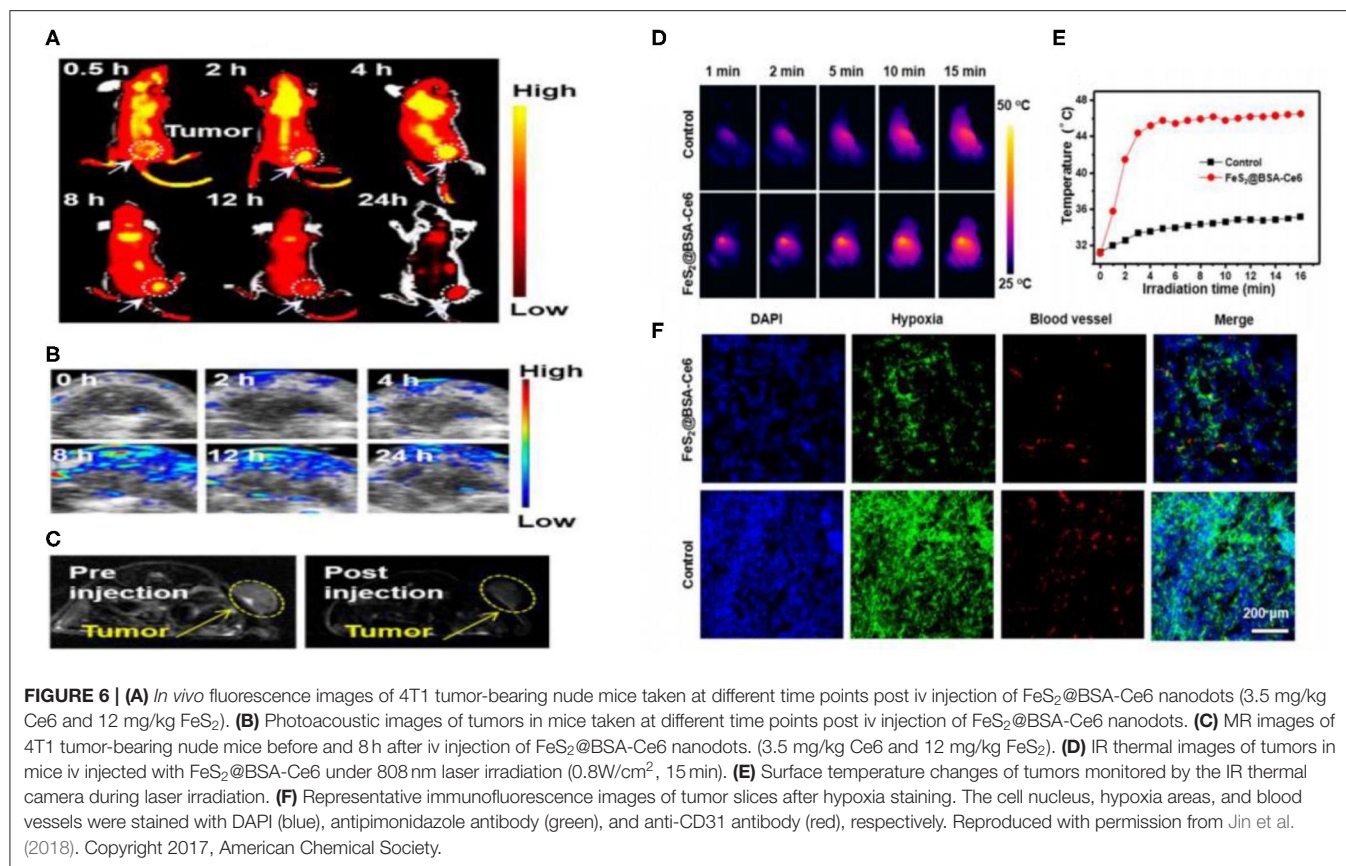
Iron sulfur clusters are critical cofactors in many enzymes and proteins which conduct redox reactions and regulate oxidative stress. Thus, nano-sized iron sulfides are expected to perform similar catalysis and act as nanozymes. Previous studies have shown that iron sulfide can effectively activate persulfate (PS) or peroxymonosulfate (PMS) to generate sulfate radicals (Xiao et al., 2020). Other common reactions involving iron sulfide are shown in section Sonochemical Synthesis. Since iron oxide nanoparticles were shown to possess intrinsic peroxidase activity in 2007 (Gao et al., 2007), it has been speculated that iron sulfide has similar properties. The catalytic processes of iron sulfide are shown in Figure 4. High catalytic activity,

multi-enzymes activities, harsh environmental resistance, storage stability, and the intrinsic advantages of nanomaterials provide further possibilities for biomedicine development, meaning that good alternatives to natural enzymes exist. The enzymatic activity of iron sulfide has been intensely investigated. In 2010, FeS nanosheets were reported to possess peroxidase-like activity. FeS suspensions were shown to catalyze the oxidation of peroxidase substrates, 3, 3', 5, 5'-Tetramethylbenzidine (TMB) to produce a blue product in the presence of H<sub>2</sub>O<sub>2</sub> (Dai et al., 2009) (Figure 4). Fe<sub>7</sub>S<sub>8</sub> nanowires' also possessing intrinsic peroxidase activity was also reported in 2013 for which catalytic behavior was observed. The apparent K<sub>M</sub> of Fe<sub>7</sub>S<sub>8</sub> with TMB as a substrate was 0.548 mM, almost six times lower than that of horseradish peroxidase (HRP). These results demonstrate that Fe<sub>7</sub>S<sub>8</sub> has a higher affinity to TMB than to HRP (Yao et al., 2013). In 2015, magnetic Fe<sub>3</sub>S<sub>4</sub> NPs was shown to possess peroxidase-like activity. Through investigating steady state kinetics, Fe<sub>3</sub>S<sub>4</sub> was shown to possess a higher affinity for H<sub>2</sub>O<sub>2</sub> than HRP. The reasons could be that Fe<sub>3</sub>S<sub>4</sub> binds to and reacts with H<sub>2</sub>O<sub>2</sub>, following which nanozyme is released prior to reacting with the second substrate TMB (Ding et al., 2016). nFeS (Fe<sub>1-x</sub>S and Fe<sub>3</sub>S<sub>4</sub>) (detailed description in section Hydrothermal Synthesis) have been shown to possess both peroxidase-like and catalase-like activity (Figure 4). nFeS is able to decompose H<sub>2</sub>O<sub>2</sub> into free radicals and O<sub>2</sub>, promoting the release of polysulfanes (Xu et al., 2018). FeS<sub>2</sub> has also been shown to possess amylase-like properties (Srivastava et al., 2014b).

## Antibacterial Alternatives

Schoonen et al. reported on the antibacterial action of FeS<sub>2</sub>. Its mechanism was shown to be related to the formation of H<sub>2</sub>O<sub>2</sub>. The same group also reported how minerals can induce the formation of reactive oxygen species (Cohn et al., 2006; Schoonen et al., 2006). The rapid absorption of Fe<sup>2+</sup> can influence bacterial metabolism. The oxidation of Fe<sup>2+</sup> to Fe<sup>3+</sup> leads to reactive oxygen species (ROS) production and biomolecular damage. As a result, iron sulfide can act as antimicrobial agents. Iron sulfides have been reported to be effective in bacterial infections. In 2013, He et al. reported on the bacteriostatic activity of Fe<sub>3</sub>S<sub>4</sub>/Ag against *E. coli* (86.2%) and *S. aureus* (90.6%). Meanwhile, Fe<sub>3</sub>S<sub>4</sub> NPs without Ag have no effect (He et al., 2013). The Arenas-Arrocena group synthesized Fe<sub>x-1</sub>S NPs and reported their antibacterial and cytotoxic activity in 2018. Antibacterial activity against *S. aureus*, *E. coli* and *E. faecalis* was observed (Argueta-Figueroa et al., 2018). In addition, Gao and coworkers discovered antibacterial inorganic iron polysulfides materials that were converted by organosulfur compounds in 2018. Inorganic nano-sulfides (nFeS, Fe<sub>1-x</sub>S, and Fe<sub>3</sub>S<sub>4</sub>) have shown inhibition against *Pseudomonas aeruginosa* and *Staphylococcus aureus*. These studies also described new strategies to synthesize iron sulfide nanomaterials. Furthermore, the *S. mutans* biofilm-related infections could be prevented by nFeS (Xu et al., 2018) (Figure 5). The antibacterial properties of FeS<sub>2</sub>-Bi<sub>2</sub>O<sub>3</sub> against the pathogenic microorganisms *Mycobacterium tuberculosis* and *Salmonella* have also been measured (Manafi et al., 2019). Diksha et al. reported that FeS NPs could enhance intrabacterial ROS levels in bacteria by light irradiation in 2020. This was revealed





as the primary antibacterial mechanism of FeS NPs (Agnihotri et al., 2020).

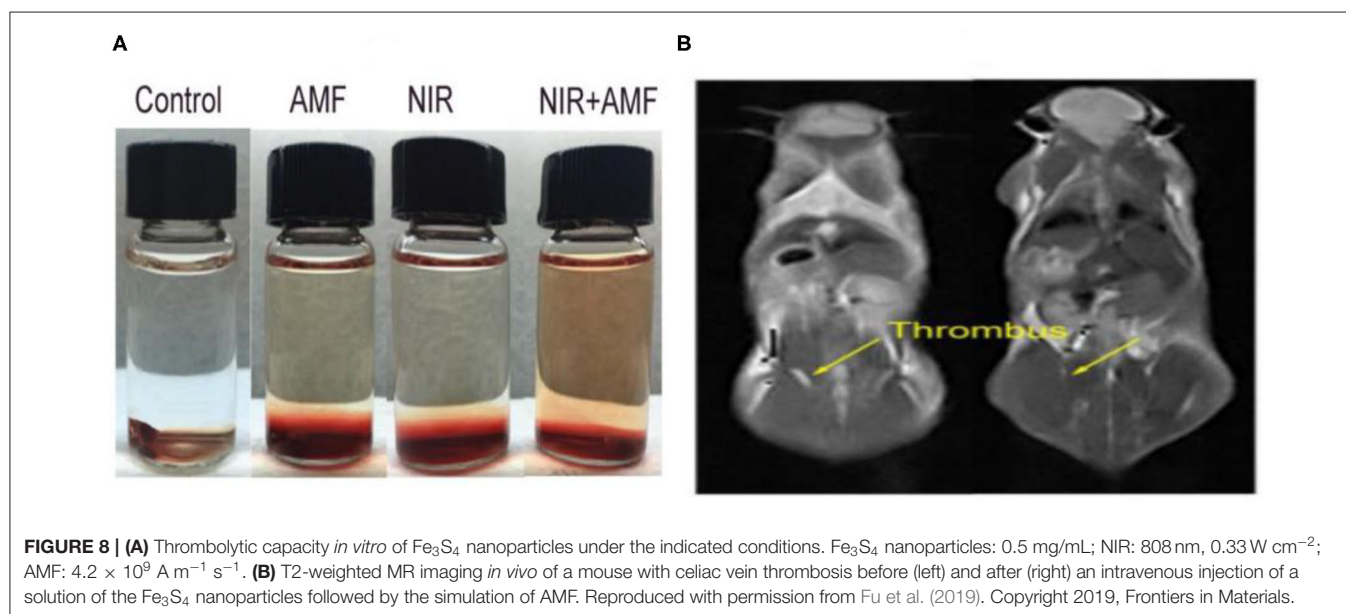
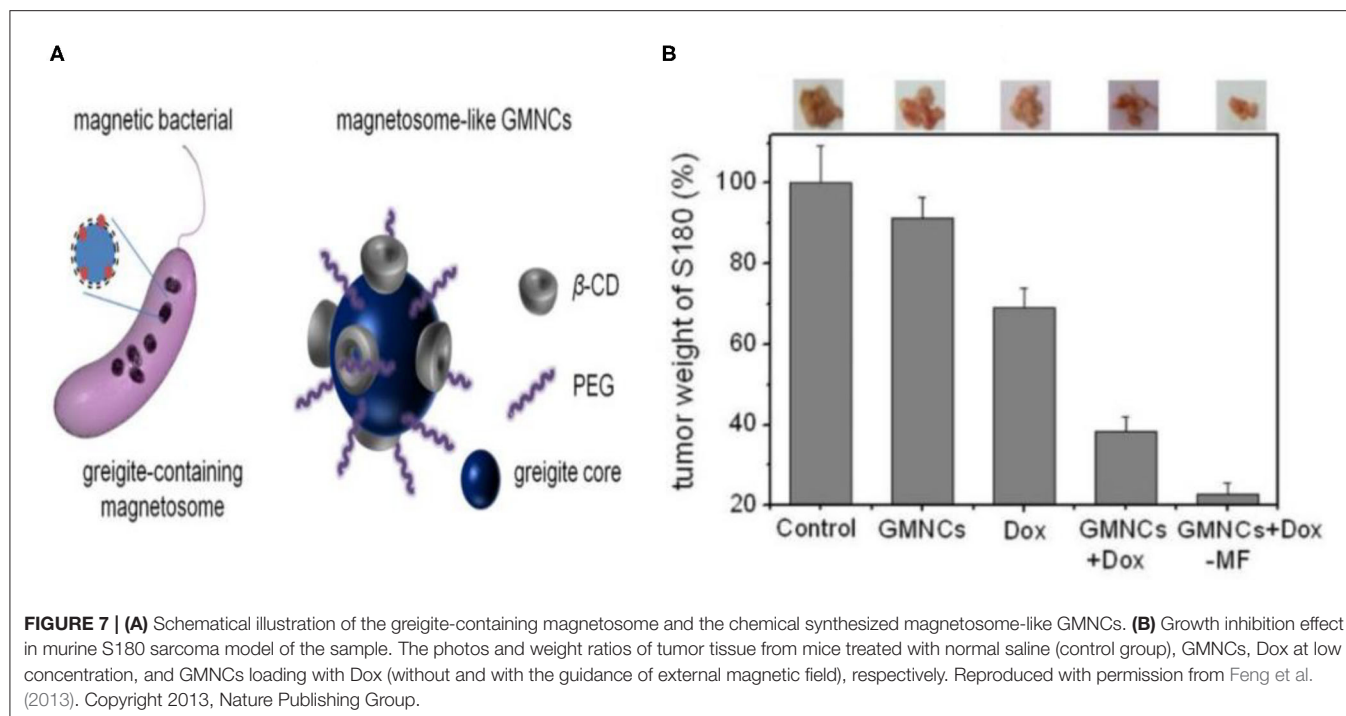
## Cancer Therapy

Chen and colleagues reported that tumors in mice could disturb iron metabolism in the major organs. The chemical form of iron in the tumors was ferrous-sulfide-like iron and ferritin, highlighting the potential of iron sulfide for cancer treatment (Chen and Chen, 2017). Chang et al. synthesized Fe<sub>3</sub>S<sub>4</sub> particles with magnetic properties through co-precipitation. The NPs were used for cancer hyperthermia providing a new avenue for multimodal anticancer therapies (Chang et al., 2011). In 2015, Yang et al. concluded that triangle nanoplates (FeS/PEG nanostructures) could be used as nanoagents for *in vivo* MRI-guided photothermal cancer treatment. High doses of FeS nanoplates were shown to be safe and effective in mice. This study highlighted the potential clinical use of FeS, for MRI in addition to PTT (Figure 6) (Yang et al., 2015). In 2018, Fe<sub>3</sub>S<sub>4</sub> nanosheets were shown to possess high efficiencies for MRI guided photothermal and chemodynamic synergistic therapy, opening up a new direction for the design of inorganic iron sulfide for future clinical applications (Guan et al., 2018). Tiny nano-sized iron sulfide with simple biomineralization method has also been attention owing to its huge potential *in vivo* application especially in cancer therapy combined with its

excellent photothermal and magnetic performance. FeS<sub>2</sub>@BSA-Ce6 (detailed in section Biomineralization) exhibited good results whether *in vivo* multimodal imaging or *in vivo* combined therapy (Jin et al., 2018). Meanwhile, the latest literature proved 3 nm FeS@BSA QDs could be used as T1-weighted MRI contrast agents. Moreover, the ultrasmall QDs showed good results in photothermal therapy and they could be cleared via glomerular filtration into bladder after treatment (Yang et al., 2020). The use of iron chalcogenides has also been investigated. Cu<sub>5</sub>FeS<sub>4</sub>-PEG NPs were effective in dual-modal imaging and PTT (Zhao et al., 2016). In 2017, CuFeS<sub>2</sub> nanoplates were used for *in vivo* photothermal/photoacoustic imaging and cancer chemotherapy/PTT (Ding et al., 2017).

## Drug Delivery

Iron sulfide holds utility as a drug carrier. In previous studies, modified  $\beta$ -cyclodextrin ( $\beta$ -CD) and PEG Fe<sub>3</sub>S<sub>4</sub> (GMNCs) were used as drug loading NPs. Both  $\beta$ -CD and PEG have been used to control the shape and size of GMNCs as surfactants. In addition, the biocompatibility of Fe<sub>3</sub>S<sub>4</sub> is enhanced, with entrapment efficiencies of 58.7% for the modified delivery of the chemotherapeutic drug doxorubicin. Meanwhile, the enhanced chemotherapeutic treatment of mouse tumors was obtained through the intravenous injection of doxorubicin (Dox) loaded GMNCs (Feng et al., 2013; Figure 7).



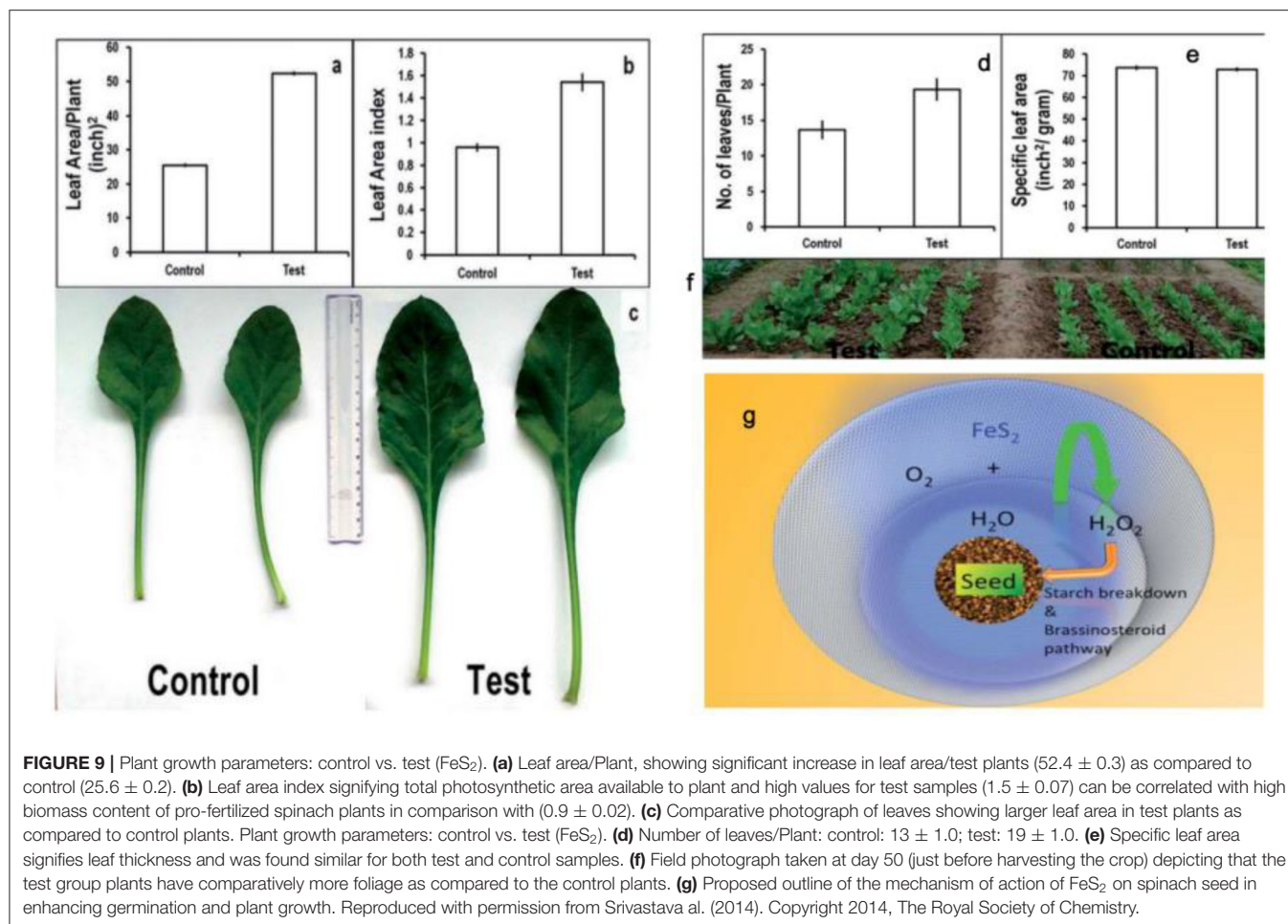
## Thrombolytic Agents

In studies of vascular disease, the removal of thrombosis through non-invasive methods is challenging. However, studies regarding iron sulfide NPs as thrombolytic agents have been reported. Ge et al. first highlighted the utility of  $\text{Fe}_3\text{S}_4$  NPs as thrombolytic agents with both photothermal and magnetothermal thrombolytic capability. Using  $\text{Fe}_3\text{S}_4$  nanoparticles, celiac vein thrombosis could be prevented using magnetic hyperthermia combined PTT. Both *in vivo* and *in vitro*,  $\text{Fe}_3\text{S}_4$  has demonstrated beneficial effects for the removal of

thrombi (Figure 8), providing a novel hyperthermia strategy for the prevention of thrombosis (Fu et al., 2019).

## Biosensors

Iron sulfides have been used as glucose sensors due to their intrinsic peroxidase-like activity (Dai et al., 2009). Glucose sensors can be developed using colorimetric methods in which cascade reactions form the core mechanism of glucose detection. TMB could be oxidized to oxTMB in the presence of glucose, GOx and iron sulfide.  $\text{H}_2\text{O}_2$  produced by the decomposition



of glucose in the presence of glucose oxidase can be used as a substrate for iron sulfide. Iron sulfide peroxidase-like mimics can oxidize TMB to oxTMB in the presence of  $\text{H}_2\text{O}_2$ .  $\text{Fe}_7\text{S}_8$  nanowires also possess peroxidase activity. Using a linear range, glucose concentrations of  $5 \times 10^{-6}$  to  $5 \times 10^{-4}$  M could be detected (Yao et al., 2013). In 2016, Xian and colleagues used  $\text{Fe}_3\text{S}_4$  magnetic nanoparticles (MNPs) to quantify glucose concentrations in human serum. A linear range was measured from 2 to 100  $\mu\text{M}$ , and the limit of detection (LOD) was 0.16  $\mu\text{M}$  (Ding et al., 2016). These studies highlighted the potential of as-prepared iron sulfide as both glucose sensors and artificial peroxidase nanozymes.

## Antifungal Agents

*In vitro* antifungal  $\text{FeS}$  NPs exhibited significant anti-fungal activity against *F. verticillioides* at 18  $\mu\text{g ml}^{-1}$ , with a higher efficiency than standard fungicides (carbendazim (median effective dose (ED50): 230  $\mu\text{g ml}^{-1}$ ). These were the first reports highlighting the antifungal activity of iron sulfide. The influence of  $\text{FeS}$  on both seed health and quality parameters of rice was also evaluated based on this antifungal activity. Iron sulfides were

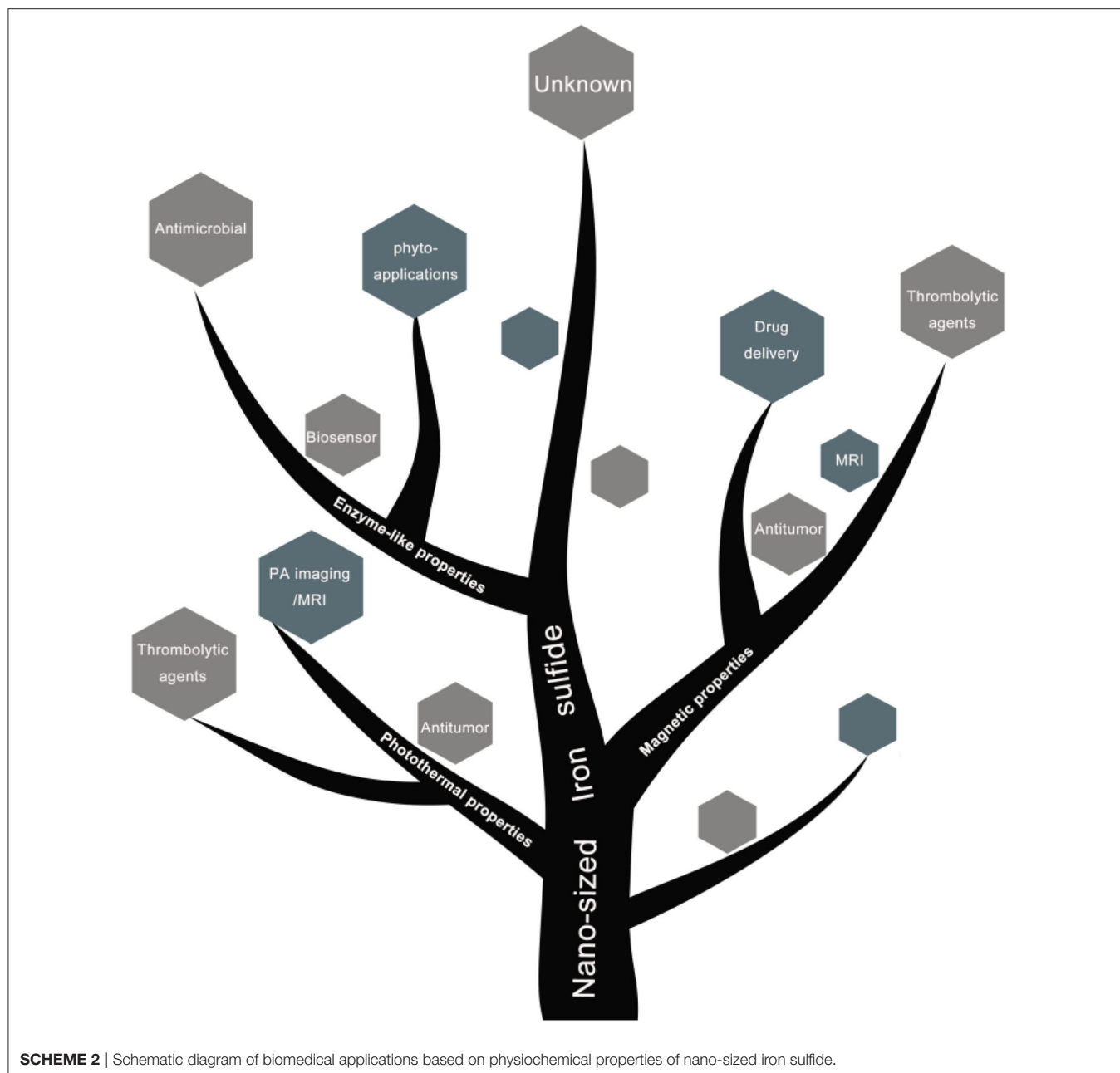
shown to be effective in iron deficient soils as an alternative to high dose organic fungicides (Ahuja et al., 2019).

## Seed Improvements in Phyto-Applications

$\text{FeS}_2$  represents a photovoltaic material, which increases plant biomass in the seeds of chickpeas (*Cicer arietinum*). Meanwhile, the mechanism of functional  $\text{FeS}_2$  is attributed to its amylase-like activity. In the presence of  $\text{H}_2\text{O}$  and  $\text{FeS}_2$ , starch in the seeds can be broken down to  $\text{H}_2\text{O}_2$ , which participates in the absorption of  $\text{CO}_2$  and improves plant health. Spinach seeds treated with  $\text{FeS}_2$  exhibited broader leaf morphologies, larger leaf numbers and an increased biomass (Srivastava et al., 2014b) (**Figure 9**). In later studies, seed priming with  $\text{FeS}_2$  was reported as an innovative strategy (Das et al., 2016).  $\text{FeS}_2$  also improved both seed yield and growth in the *Brassica juncea* field (Rawat et al., 2017).

## CONCLUSIONS

In summary, we have highlighted the most recent methods of nano-iron sulfide synthesis, including nano iron sulfide modifications and characterizations. Strikingly, nano-sized iron sulfides demonstrate versatile physiochemical properties,



enzyme-like catalysis, high stability and biocompatibility, which facilitate their biomedical applications. A range of nano-iron sulfides have been assessed in catalysis, tumor therapy, antibacterials and antifungals, drug delivery, biosensors, thrombus removal and in plants. Their advantages include (1) high biocompatibility due to the key role of iron and sulfur in natural life; (2) the photothermal and magnetic properties of nano-sized iron sulfide; (3) their nanostructure and large surface area that can improve drug delivery; and (4) their enzyme-like properties as nanozymes, including their high reactivity to numerous chemical substances that can regulate

hydrogen peroxide, ROS and various catalytic reactions to treat related diseases.

Although it has been shown that nano-sized iron sulfides represent great potential in numerous applications in biomedicine (Scheme 2), a number of issues remain to be addressed, including the synthesis of iron sulfide that is stable and in a single phase, with modifications to adapt to the biological environment. Studies have found that the modification of molecular CTAB inhibits the preparation of  $\text{Fe}_3\text{S}_4$  NPs due to competitive inhibition with  $\text{Na}_2\text{S}$  under acidic conditions, resulting in the formation of non-magnetic iron sulfides and

other byproducts. Citrate modified nanoparticles have not sufficient particle spacing due to aggregation effects (Simeonidis et al., 2016). In addition, the biomedical assessments of iron sulfides remain sparse, and their mechanisms of action under physiological conditions are poorly understood. The intrinsic enzyme-like properties of iron sulfide as nanozymes may provide a window to understand its biological effects and potential cytotoxicity *in vivo*. Taken together, nano-sized iron sulfides possess versatile physiochemical properties and enzyme-like properties, which describe a form of distinctive nanomaterials with great potential for use in biomedical applications.

## REFERENCES

- Agnihotri, S., Mohan, T., Jha, D., Gautam, H., and Roy, I. (2020). Dual Modality FeS Nanoparticles with Reactive Oxygen Species-Induced and Photothermal Toxicity toward Pathogenic Bacteria. *ACS OMEGA* 5, 597–602. doi: 10.1021/acsomega.9b03177
- Ahuja, R., Sidhu, A., and Bala, A. (2019). Synthesis and evaluation of iron(ii) sulfide aqua nanoparticles (FeS-NPs) against *Fusarium verticillioides* causing sheath rot and seed discoloration of rice. *Eur. J. Plant Pathol.* 155, 163–171. doi: 10.1007/s10658-019-01758-3
- Argueta-Figueroa, L., Martinez-Alvarez, O., Santos-Cruz, J., Garcia-Contreras, R., Acosta-Torres, L. S., Fuente-Hernández, J., et al. (2017). Nanomaterials made of non-toxic metallic sulfides: a systematic review of their potential biomedical applications. *Mater. Sci. Eng. C* 76, 1305–1315. doi: 10.1016/j.msec.2017.02.120
- Argueta-Figueroa, L., Torres-Gómez, N., García-Contreras, R., Vilchis-Nestor, A. R., Martínez-Alvarez, O., Acosta-Torres, L. S., et al. (2018). Hydrothermal synthesis of pyrrhotite (Fe<sub>x-1</sub>S) nanoplates and their antibacterial, cytotoxic activity study. *Progress Nat. Sci.* 28, 447–455. doi: 10.1016/j.pnsc.2018.06.003
- Barand, A., and Russo, S. (2009). Modeling the environmental stability of FeS<sub>2</sub> nanorods, using lessons from biomineralization. *Nanotechnology* 20:115702. doi: 10.1088/0957-4484/20/11/115702
- Barnard, A., and Russo, S. (2009). Morphological stability of Pyrite FeS<sub>2</sub> nanocrystals in water. *J. Phys. Chem. C* 113, 5376–5380. doi: 10.1021/jp809377s
- Beal, J., Etchegoin, P., and Tilley, R. (2012). Synthesis and characterisation of magnetic iron sulfide nanocrystals. *J. Solid State Chem.* 189, 57–62. doi: 10.1016/j.jssc.2012.01.015
- Bi, Y., Yuan, Y., Exstrom, C. L., Darveau, S. A., and Huang, J. (2011). Air stable, photosensitive, phase pure iron pyrite nanocrystal thin films for photovoltaic application. *Nano Letter* 11, 4953–4957. doi: 10.1021/nl202902z
- Chang, Y., Savitha, S., Sadhasivam, S., Hsu, C., and Lin, F. (2011). Fabrication, characterization, and application of greigite nanoparticles for cancer hyperthermia. *J. Colloid Interface Sci.* 363, 314–319. doi: 10.1016/j.jcis.2010.06.069
- Chen, R., and Chen, G. (2017). Tumor-induced disorder of iron metabolism in major organs: a new insight from chemical speciation of iron. *J. Int. Med. Res.* 46, 70–78. doi: 10.1177/0300060517718711
- Chen, B., and Gu, N. (2017). Current status and development of pharmaceutical iron based nanomaterials. *Mater. China* 36, 211–218.
- Cohn, C., Laffers, R., Simon, S., O'Riordan, T., and Schoonen, M. (2006). Role of pyrite in formation of hydroxyl radicals in coal: possible implications for human health. *Part. Fibre Toxicol.* 3:16. doi: 10.1186/1743-8977-3-16
- Dai, Z., Liu, S., Bao, J., and Ju, H. (2009). Nanostructured FeS as a mimic peroxidase for biocatalysis and biosensing. *Chem. Eur. J.* 15, 4321–4326. doi: 10.1002/chem.200802158
- Das, C., Srivastava, G., Dubey, A., Roy, M., Jain, S., Sethy, N., et al. (2016). Nano-ironpyrite seed dressing: A sustainable intervention to reduce fertilizer consumption in vegetable (beetroot, carrot), spice (fenugreek), fodder (alfalfa), and oilseed (mustard, sesamum) crops. *Nanotechnol. Environ. Eng.* 1, 1–12. doi: 10.1007/s41204-016-0002-7
- Davison, W. (1991). The solubility of iron sulphides in synthetic and natural waters at ambient temperature. *Aquatic Sci.* 53, 309–329. doi: 10.1007/BF00877139
- ## AUTHOR CONTRIBUTIONS
- All authors listed have made a substantial, direct and intellectual contribution to the work, and approved it for publication.
- ## ACKNOWLEDGMENTS
- This work was supported by the National Key R&D Program of China (Grant No. 2018YFC1003500), as well as the National Natural Science Foundation of China (Grant Nos. 81930050, 81671810, and 31701236).
- De Leeuw, N., Parker, S., Sithole, H., and Ngoepe, P. E. (2000). Modeling the surface structure and reactivity of pyrite: introducing a potential model for FeS<sub>2</sub>. *J. Phys. Chem. B* 104, 7969–7976. doi: 10.1021/jp0009498
- Ding, B., Yu, C., Li, C., Deng, X., Ding, J., Cheng, Z., et al. (2017). Cis-platinum pro-drug-attached CuFeS<sub>2</sub> nanoplates for *in vivo* photothermal/photoacoustic imaging and chemotherapy/photothermal therapy of cancer. *Nanoscale* 9, 16937–16949. doi: 10.1039/C7NR04166G
- Ding, C., Yan, Y., Xiang, D., Zhang, C., and Xian, Y. (2016). Magnetic Fe<sub>3</sub>S<sub>4</sub> nanoparticles with peroxidase-like activity, and their use in a photometric enzymatic glucose assay. *Microchim. Acta* 183, 625–631. doi: 10.1007/s00604-015-1690-6
- Dong, H., Fan, Y., Zhang, W., Gu, N., and Zhang, Y. (2019). Catalytic mechanisms of nanozymes and their applications in biomedicine. *Bioconjug. Chem.* 30, 1273–1296. doi: 10.1021/acs.bioconjugchem.9b00171
- Elliot, A. (2010). Structure of pyrrhotite 5c (Fe<sub>9</sub>S<sub>10</sub>). *Acta Crystallogr. Section B* 66, 271–279. doi: 10.1107/S0108768110011845
- Esmaili, E., Eslami-Arshaghi, T., Hosseinzadeh, S., Elahirad, E., Jamalpoor, Z., Hatamie, S., et al. (2020). The biomedical potential of cellulose acetate/polyurethane nanofibrous mats containing reduced graphene oxide/silver nanocomposites and curcumin: antimicrobial performance and cutaneous wound healing. *Int. J. Biol. Macromol.* 152, 418–427. doi: 10.1016/j.ijbiomac.2020.02.295
- Feng, M., Lu, Y., Yang, Y., Zhang, M., Xu, Y., Gao, H., et al. (2013). Bioinspired greigite magnetic nanocrystals: chemical synthesis and biomedicine applications. *Sci. Rep.* 3:994. doi: 10.1038/srep02994
- Fleet, M. (1971). The crystal structure of a pyrrhotite (Fe<sub>7</sub>S<sub>8</sub>). *Acta Cryst. B* 27:1864. doi: 10.1107/S0567740871004990
- Fu, D., Liu, J., Ren, Q., Ding, J., Ding, H., Chen, X., et al. (2019). magnetic iron sulfide nanoparticles as thrombolytic agents for magnetocaloric therapy and photothermal therapy of thrombosis. *Front. Mater.* 6:316. doi: 10.3389/fmats.2019.00316
- Gan, Y., Xu, F., Luo, J., Yuan, H., Jin, C., Zhang, L., et al. (2016). One-pot biotemplate synthesis of FeS<sub>2</sub> decorated sulfur-doped carbon fiber as high capacity anode for lithium-ion batteries. *Electrochim. Acta* 209, 201–209. doi: 10.1016/j.electacta.2016.05.076
- Ganbaatar, N., Matsuzaki, N., Nakazawa, Y., Afrin, R., Aono, M., Yano, T., et al. (2016). Surface force analysis of pyrite (FeS<sub>2</sub>): its reactivity to amino acid adsorption. *Adv. Mater. Phys. Chem.* 6, 167–176. doi: 10.4236/ampc.2016.67018
- Gao, L., Zhuang, J., Nie, L., Zhang, J., Zhang, Y., Gu, N., et al. (2007). Intrinsic peroxidase-like activity of ferromagnetic nanoparticles. Intrinsic peroxidase-like activity of ferromagnetic nanoparticles. *Nat. Nanotechnol.* 2, 577–583. doi: 10.1038/nnano.2007.260
- Gao, S., Huang, F., Song, D., Li, G., Liu, Q., Feng, T., et al. (2015). “Growth mechanism and stability study on the Fe<sub>3</sub>S<sub>4</sub> nanocrystals synthesized under thermal and humid conditions,” in *Proceedings of the 11th International Congress for Applied Mineralogy*. doi: 10.1007/978-3-319-13948-7\_13
- Guan, G., Wang, X., Li, B., Zhang, W., Cui, Z., Lu, X., et al. (2018). “Transformed” Fe<sub>3</sub>S<sub>4</sub> tetragonal nanosheets: a high-efficiency and body-clearable agent for magnetic resonance imaging guided photothermal and chemodynamic synergistic therapy. *Nanoscale* 10, 17902–17911. doi: 10.1039/C8NR06507A

- Guo, S., Li, J., Ma, Z., Chi, Y., and Xue, H. (2016). A facile method to prepare FeS/porous carbon composite as advanced anode material for lithium-ion batteries. *J. Mater. Sci.* 52, 2345–2355. doi: 10.1007/s10853-016-0527-y
- Guo, Z., Sun, F., Han, B., Lin, K., Zhou, L., and Yuan, W. (2017). Iron vacancy in tetragonal Fe<sub>1-x</sub>S crystals and its effect on the structure and superconductivity. *Phys. Chem. Chem. Phys.* 19, 9000–9006. doi: 10.1039/C7CP00068E
- He, Q., Huang, C., and Liu, J. (2013). Preparation, Characterization and antibacterial activity of magnetic greigite and Fe<sub>3</sub>S<sub>4</sub>/Ag nanoparticles. *Nanosci. Nanotechnol. Lett.* 5, 1–8. doi: 10.1166/nnl.2014.1727
- He, Y., Wilson, J., Su, C., and Wilkin, R. T. (2015). Review of abiotic degradation of chlorinated solvents by reactive iron minerals in aquifers. *Ground Water Monitoring Remediation* 35, 57–75. doi: 10.1111/gwmr.12111
- Jin, A., Mi-Ju, K., Kug-Seung, L., Yu, S., and Sung, Y. (2019). Spindle-like Fe<sub>7</sub>S<sub>8</sub>/N-doped carbon nanohybrids for high-performance sodium ion battery anodes. *Nano Res.* 12, 695–700. doi: 10.1007/s12274-019-2278-y
- Jin, J., Wu, W., Min, H., Wu, H., Wang, S., Ding, Y., et al. (2017). A glassy carbon electrode modified with FeS nanosheets as a highly sensitive amperometric sensor for hydrogen peroxide. *Microchim. Acta* 184, 1389–1396. doi: 10.1007/s00604-017-2105-7
- Jin, Q., Liu, J., Zhu, W., Dong, Z., Liu, Z., and Cheng, L. (2018). Albumin-assisted synthesis of ultrasmall FeS<sub>2</sub> nanodots for imaging-guided photothermal enhanced photodynamic therapy. *ACS Appl. Mater. Interfaces* 10, 332–340. doi: 10.1021/acsami.7b16890
- Kar, S., and Chaudhuri, S. (2004). Solvothermal synthesis of nanocrystalline FeS<sub>2</sub> with different morphologies. *Chem. Phys. Lett.* 398, 22–26. doi: 10.1016/j.cplett.2004.09.028
- Kasting, J. (1993). Earth's early atmosphere. *Science* 259, 920–926. doi: 10.1126/science.11536547
- Kavner, A., Duffy, T., and Shen, G. (2001). Phase stability and density of FeS at high pressures and temperatures: implications for the interior structure of Mars. *Earth Planet. Sci. Lett.* 185, 25–33. doi: 10.1016/S0012-821X(00)00356-3
- Kim, E. J., and Batchelor, B. (2009). Synthesis and characterization of pyrite (FeS<sub>2</sub>) using microwave irradiation. *Mater. Res. Bull.* 44, 1553–1558. doi: 10.1016/j.materresbull.2009.02.006
- Kong, X., Lou, T., and Li, Y. (2005). Fe<sub>7</sub>S<sub>8</sub> nanorods and nanosheets. *J. Alloys Compd.* 390, 236–239. doi: 10.1016/j.jallcom.2004.07.054
- Kuhn, S. J., Eskildsen, M. R., Debeer-Schmitt, L., Li, L., de La Cruz, C., and Sefat, A. S. (2016). Structure and magnetic interactions in FeS: a low-Tc superconductor. *Bull. Am. Phys. Soc.* 61, 2. Abstracts retrieved from APS March Meeting (Abstract ID: BAPS.2016.MAR.H11.12).
- Kwon, K., Refson, K., Bone, S., Qiao, R., Yang, W., Liu, Z., et al. (2011). Magnetic ordering in tetragonal FeS: evidence for strong itinerant spin fluctuations. *Phys. Rev. B Cond. Matt.* 83, 064402.1–064402.7. doi: 10.1103/PhysRevB.83.064402
- Lefèvre, C., Abreu, F., Lins, U., and Bazylinski, D. (2010). Nonmagnetotactic multicellular prokaryotes from low-saline, nonmarine aquatic environments and their unusual negative phototactic behavior. *Appl. Environ. Microbiol.* 76, 3220–3227. doi: 10.1128/AEM.00408-10
- Li, M., Yao, Q., Zhou, G., Qu, X., Mu, C., and Fu, S. (2011). Microwave-assisted controlled synthesis of monodisperse pyrite microspherulites. *Cryst. Eng. Comm.* 13, 5936–5942. doi: 10.1039/c1ce05478c
- Li, X., Xu, H., Chen, Z., Chen, Z., and Chen, G. (2011). Biosynthesis of nanoparticles by microorganisms and their applications. *J. Nanomater.* 2011, 1–16. doi: 10.1155/2011/270974
- Li, Y., Pu, Q., Li, S., Zhang, H., Wang, X., Yao, H., et al. (2019). Machine learning methods for research highlight prediction in biomedical effects of nanomaterial application. *Patt. Recognit. Lett.* 117, 111–118. doi: 10.1016/j.patrec.2018.11.008
- Liang, M., and Yan, X. (2019). Nanozymes: from new concepts, mechanisms, and standards to applications. *Acc. Chem. Res.* 52, 2190–2200. doi: 10.1021/acs.accounts.9b00140
- Ma, J., Chang, L., Lian, J., Huang, Z., Duan, X., Liu, X., et al. (2010). Ionic liquid-modulated synthesis of ferrimagnetic Fe<sub>3</sub>S<sub>4</sub> hierarchical superstructures. *Chem. Commun.* 46, 5006–5008. doi: 10.1039/c0cc00479k
- Manafi, A., Hosseini, M., Fakhri, A., Gupta, V., and Agarwal, S. (2019). Investigation of photocatalytic process for iron disulfide-bismuth oxide nanocomposites by using response surface methodology: structural and antibacterial properties. *J. Mol. Liq.* 289:110950. doi: 10.1016/j.molliq.2019.110950
- Mann, S., Sparks, N., Frankel, R., Bazylinski, D., and Jannasch, H. (1990). Biomineralization of ferrimagnetic greigite (Fe<sub>3</sub>S<sub>4</sub>) and iron pyrite (FeS<sub>2</sub>) in a magnetotactic bacterium. *Nature* 343, 258–261. doi: 10.1038/343258a0
- Mei, B., and Ma, Z. (2013). Study of anti-friction performance of spherical FeS nanoparticle. *Appl. Mech. Mater.* 475–476, 1334–1339. doi: 10.4028/www.scientific.net/AMM.475-476.1334
- Menyeh, A., and O'Reilly, W. (1997). Magnetic hysteresis properties of fine particles of monoclinic pyrrhotite Fe<sub>7</sub>S<sub>8</sub>. *J. Geomag. Geoelectr.* 49, 965–976. doi: 10.5636/jgg.49.965
- Mofokeng, T., Mabena, G., Moloto, M. J., Shumbula, P. M., Mubiayi, P., and Nyamukamba, P. (2017). Temperature influence on the lactose capped metal sulphide nanoparticles. *Chalcogenide Lett.* 14, 347–355.
- Mohindar, S., and Jagadeesh, M. (1979). Temperature-dependent magnetic susceptibility of marcasite (FeS<sub>2</sub>). *Phys. Rev. B* 20:3897. doi: 10.1103/PhysRevB.20.3897
- Moore, J., Nienhuis, E., Ahmadzadeh, M., and McCloy, J. (2019). Synthesis of greigite (Fe<sub>3</sub>S<sub>4</sub>) particles via a hydrothermal method. *AIP Adv.* 9:035012. doi: 10.1063/1.5079759
- Niño, M., Flores, E., Sanchez, C., and Rojo, J. (2018). Reactivity of a FeS surface under room temperature exposure to nitrogen and H<sub>2</sub>S. *J. Phys. Chem. B* 122, 705–712. doi: 10.1021/acs.jpcc.7b06309
- Ono, S. (2007). Magnetic phase transition of FeS at high pressures. *Acta Crystallogr. Sect. A Found. Crystallogr.* 63:59. doi: 10.1107/S0108767307098716
- Paoletta, A., George, C., Povia, M., Zhang, Y., Krahne, R., Gich, M., et al. (2011). Charge transport and electrochemical properties of colloidal greigite (Fe<sub>3</sub>S<sub>4</sub>) nanoplatelets. *Chem. Mater.* 23, 3762–3768. doi: 10.1021/cm201531h
- Powell, A. V., Vaqueiro, P., Knight, K. S., Chapon, L. C., and Sánchez, R. D. (2004). Structure and magnetism in synthetic pyrrhotite Fe<sub>7</sub>S<sub>8</sub>: a powder neutron-diffraction study. *Phys. Rev. B* 70, 014415. doi: 10.1103/PhysRevB.70.014415
- Qi, W., and Cowan, J. (2011). Structural, mechanistic and coordination chemistry of relevance to the biosynthesis of iron–sulfur and related iron cofactors. *Coord. Chem. Rev.* 255, 688–699. doi: 10.1016/j.ccr.2010.10.016
- Rawat, M., Nayan, R., Negi, B., Zaidi, M. G. H., and Arora, S. (2017). Physio-biochemical basis of iron-sulfide nanoparticle induced growth and seed yield enhancement in b. juncea. *Plant Physiol. Biochem.* 118, 274–284. doi: 10.1016/j.plaphy.2017.06.021
- Rickard, D. (2006). The solubility of FeS. *Geochim. Cosmochim. Acta* 70, 5779–5789. doi: 10.1016/j.gca.2006.02.029
- Rickard, D., and Luther, G. (2007). Chemistry of iron sulfides. *Chem. Rev.* 107, 514–562. doi: 10.1021/cr0503658
- Roberts, A. (1995). Magnetic properties of sedimentary greigite (Fe<sub>3</sub>S<sub>4</sub>). *Earth Planetary Sci. Lett.* 134, 227–236. doi: 10.1016/0012-821X(95)00131-U
- SantosCarballal, D., Roldan, A., Dzade, N., and de Leeuw, N. H. (2017). Reactivity of CO<sub>2</sub> on the surfaces of magnetite (Fe<sub>3</sub>O<sub>4</sub>), greigite (Fe<sub>3</sub>S<sub>4</sub>) and mackinawite (FeS). *Philos. Trans. R. Soc. A* 376:65. doi: 10.1098/rsta.2017.0065
- Scaini, M., Bancroft, G., and Knipe, S. (1998). Reactions of aqueous Au<sup>1+</sup> sulfide species with pyrite as a function of pH and temperature. *Am. Mineral.* 83, 316–322. doi: 10.2138/am-1998-3-415
- Schoonen, M., Cohn, C., Roemer, E., Laffers, R., Simon, S., and O'Riordan, T. (2006). Mineral-induced formation of reactive oxygen species. *Med. Mineralo. Geochem.* 64, 179–221. doi: 10.2138/rmg.2006.64.7
- Simeonidis, K., Liébana-Viñas, S., Wiedwald, U., Ma, Z., Li, Z.-A., Spasova, M., et al. (2016). A versatile large-scale and green process for synthesizing magnetic nanoparticles with tunable magnetic hyperthermia features. *RSC Adv.* 6, 53107–53117. doi: 10.1039/C6RA09362K
- Snowball, I. (1991). Magnetic hysteresis properties of greigite (Fe<sub>3</sub>S<sub>4</sub>) and a new occurrence in holocene sediments from swedish lapland. *Phys. Earth Planetary Interiors* 68, 32–40. doi: 10.1016/0031-9201(91)90004-2
- Srivastava, G., Das, A., Kusurkar, T., Roy, M., Airan, S., Sharma, R., et al. (2014a). Ironpyrite, a potential photovoltaic material, increases plant biomass upon seed pretreatment. *Mater. Express* 4, 23–31. doi: 10.1166/mex.2014.1139
- Srivastava, G., Das, C. K., Das, A., Singh, S., Roy, M., Kim, H., et al. (2014b). Seed treatment with iron pyrite (FeS<sub>2</sub>) nanoparticles increases the production of spinach. *RSC Adv.* 4, 58495–58504. doi: 10.1039/C4RA06861K
- Usher, C., Paul, K., Narayansamy, J., Kubicki, J., Sparks, D., Schoonen, M., et al. (2005). Mechanistic aspects of pyrite oxidation in an oxidizing gaseous environment: an *in situ* HATR-IR isotope study. *Environ. Sci. Technol.* 39, 7576–7584. doi: 10.1021/es0506657

- Vanitha, P., and O'Brien, P. (2008). Phase Control In The Synthesis Of Magnetic iron sulfide nanocrystals from a cubane-type Fe-S cluster. *J. Am. Chem. Soc.* 130, 17256–17257. doi: 10.1021/ja8078187
- Wadia, C., Wu, Y., Gul, S., Volkman, S., Guo, J., and Paul Alivisatos, A. (2009). Surfactant-assisted hydrothermal synthesis of single phase pyrite FeS<sub>2</sub> nanocrystals. *Chem. Mater.* 21, 2568–2570. doi: 10.1021/cm901273v
- Wang, X., Zhou, W., Zhou, Z., An, Y., and Wu, S. (2013). Shape-controlled synthesis of iron sulfide nanostructures by thermal decomposition of organometallic precursors. *Mater. Sci. Semicond. Proc.* 16, 530–536. doi: 10.1016/j.mssp.2012.10.002
- Wang, Z., Hu, T., Liang, R., and Wei, M. (2020). Application of zero-dimensional nanomaterials in biosensing. *Front. Chem.* 8:320. doi: 10.3389/fchem.2020.00320
- Watson, J., Cressey, B., Roberts, A., Ellwood, D. C., Charnock, J., and Soper, A. K. (2000). Structural and magnetic studies on heavy-metal-adsorbing iron sulphide nanoparticles produced by sulphate-reducing bacteria. *J. Magn. Magn. Mater.* 214, 13–30. doi: 10.1016/S0304-8853(00)00025-1
- Watson, J., Ellwood, D., Deng, Q., Mikhailovsky, S., Hayter, C. E., and Evans, J. (1995). Heavy metal adsorption on bacterially produced FeS. *Minerals Eng.* 8, 1097–1108. doi: 10.1016/0892-6875(95)00075-2
- Watson, J., Ellwood, D., Soper, A., and Charnock, J. (1999). Nanosized strongly-magnetic bacterially-produced iron sulfide materials. *J. Magnetism Magnetic Mater.* 203, 69–72. doi: 10.1016/S0304-8853(99)00191-2
- Wei, H., and Wang, E. (2013). Nanomaterials with enzyme-like characteristics (nanozymes): next-generation artificial enzymes. *Chem. Soc. Rev.* 42, 6060–6093. doi: 10.1039/c3cs35486e
- Xiao, S., Cheng, M., Zhong, H., Liu, Z., Liu, Y., Yang, X., et al. (2020). Iron-mediated activation of persulfate and peroxymonosulfate in both homogeneous and heterogeneous ways: a review. *Chem. Eng. J.* 384:123265. doi: 10.1016/j.cej.2019.123265
- Xie, J., Zhang, X., Wang, H., Zheng, H., Huang, Y., and Xie, J. (2012). Analytical and environmental applications of nanoparticles as enzyme mimetics. *Trac Trends Analyt. Chemistry* 39, 114–129. doi: 10.1016/j.trac.2012.03.021
- Xu, Z., Qiu, Z., Liu, Q., Huang, Y., Li, D., Shen, X., et al. (2018). Converting organosulfur compounds to inorganic polysulfides against resistant bacterial infections. *Nat. Commun.* 9:3713. doi: 10.1038/s41467-018-06164-7
- Yang, K., Yang, G., Chen, L., Cheng, L., Wang, L., Ge, C., et al. (2015). FeS nanoplates as a multifunctional nano-theranostic for magnetic resonance imaging guided photothermal therapy. *Biomaterials* 38, 1–9. doi: 10.1016/j.biomaterials.2014.10.052
- Yang, W., Xiang, C., Xu, Y., Chen, S., Zeng, W., Liu, K., et al. (2020). Albumin-constrained large-scale synthesis of renal clearable ferrous sulfide quantum dots for T1-Weighted MR imaging and phototheranostics of tumors. *Biomaterials* 255:120186. doi: 10.1016/j.biomaterials.2020.120186
- Yao, W., Zhu, H., Li, W., Yao, H., Wu, Y., and Yu, S. (2013). Intrinsic peroxidase catalytic activity of Fe<sub>7</sub>S<sub>8</sub> nanowires templated from [Fe<sub>16</sub>S<sub>20</sub>]/diethylenetriamine hybrid nanowires. *Chem. Plus Chem.* 78, 723–727. doi: 10.1002/cplu.201300075
- Yosida, K. (1951). Note on the magnetic properties of the FeS<sub>n</sub> system. *Progr. Theor. Phys.* 6, 356–365. doi: 10.1143/ptp/6.3.356
- Zhang, L., and Webster, T. (2009). Nanotechnology and nanomaterials: promises for improved tissue regeneration. *Nano Today* 4, 66–80. doi: 10.1016/j.nantod.2008.10.014
- Zhang, M., Cui, Z., and Jiang, H. (2018). Relative stability of FeS<sub>2</sub> polymorphs with the random phase approximation approach. *J. Mater. Chem. A* 6:6606. doi: 10.1039/C8TA00759D
- Zhao, Q., Yi, X., Li, M., Zhong, X., Shi, Q., and Yang, K. (2016). High near-infrared absorbing Cu<sub>5</sub>FeS<sub>4</sub> nanoparticles for dual-modal imaging and photothermal therapy. *Nanoscale* 8, 13368–13376. doi: 10.1039/C6NR04444A

**Conflict of Interest:** The authors declare that the research was conducted in the absence of any commercial or financial relationships that could be construed as a potential conflict of interest.

Copyright © 2020 Yuan, Wang and Gao. This is an open-access article distributed under the terms of the Creative Commons Attribution License (CC BY). The use, distribution or reproduction in other forums is permitted, provided the original author(s) and the copyright owner(s) are credited and that the original publication in this journal is cited, in accordance with accepted academic practice. No use, distribution or reproduction is permitted which does not comply with these terms.